



Search for supersymmetry in pp collisions at $\sqrt{s} = 13$ TeV with 137 fb^{-1} in final states with a single lepton using the sum of masses of large-radius jets

The CMS Collaboration*

Abstract

Results are reported from a search for new physics beyond the standard model in proton-proton collisions in final states with a single lepton; multiple jets, including at least one jet tagged as originating from the hadronization of a bottom quark; and large missing transverse momentum. The search uses a sample of proton-proton collision data at $\sqrt{s} = 13$ TeV, corresponding to 137 fb^{-1} , recorded by the CMS experiment at the LHC. The signal region is divided into categories characterized by the total number of jets, the number of bottom quark jets, the missing transverse momentum, and the sum of masses of large-radius jets. The observed event yields in the signal regions are consistent with estimates of standard model backgrounds based on event yields in the control regions. The results are interpreted in the context of simplified models of supersymmetry involving gluino pair production in which each gluino decays into a top quark-antiquark pair and a stable, unobserved neutralino, which generates missing transverse momentum in the event. Scenarios with gluino masses up to about 2150 GeV are excluded at 95% confidence level (or more) for neutralino masses up to 700 GeV. The highest excluded neutralino mass is about 1250 GeV, which holds for gluino masses around 1850 GeV.

"Published in Physical Review D as doi:10.1103/PhysRevD.101.052010."

1 Introduction

The physics program of the CMS experiment at the CERN LHC [1] is designed to explore the TeV energy scale and to search for new particles and phenomena beyond the standard model (SM), for example, those predicted by supersymmetry (SUSY) [2–9]. The search described here focuses on an important experimental signature that is also strongly motivated by SUSY phenomenology. This signature includes a single lepton (an electron or a muon); several jets, arising from the hadronization of energetic quarks and gluons; at least one b-tagged jet, indicative of processes involving third-generation quarks; and \vec{p}_T^{miss} , the missing momentum in the direction transverse to the beam. A large value of $p_T^{\text{miss}} \equiv |\vec{p}_T^{\text{miss}}|$ can arise from the production of high-momentum, weakly interacting particles that escape detection. Searches for SUSY in the single-lepton final state have been performed by both ATLAS and CMS in proton-proton (pp) collisions at $\sqrt{s} = 7, 8,$ and 13 TeV [10–19].

This paper describes the single-lepton SUSY search based on the mass variable M_J , defined as the sum of the masses of large-radius jets in the event, as well as on several other kinematic variables. The search uses the combined CMS Run 2 data sample from 2016, 2017, and 2018, corresponding to a total integrated luminosity of approximately 137 fb^{-1} at $\sqrt{s} = 13$ TeV. The analysis is based on well-tested methods described in detail in two published studies [17, 19], which used Run 2 data samples of 2.3 fb^{-1} (2015) and 35.9 fb^{-1} (2016). In this version of the analysis, the signal and control region definitions have been reoptimized to take advantage of the significant increase in the size of the data sample and to maximize the analysis sensitivity to the SUSY models considered. Other improvements, such as a more advanced b tagging algorithm, have also been incorporated into the analysis.

In models based on SUSY, new particles are introduced such that all fermionic (bosonic) degrees of freedom in the SM are paired with corresponding bosonic (fermionic) degrees of freedom in the extended, supersymmetric theory. The discovery of a Higgs boson at a low mass [20–25] highlighted a key motivation for SUSY, referred to as the gauge hierarchy problem [26–31]. Assuming that the Higgs boson is a fundamental (noncomposite) spin-0 particle, its mass is subject to large quantum loop corrections, which would drive the mass up to the cutoff scale of validity of the theory. If the SM is valid up to the Planck scale associated with quantum gravity, these corrections would be enormous. Stabilizing the Higgs boson mass at a low value, without invoking extreme fine tuning of parameters to cancel the corrections, is a major theoretical challenge, which can be addressed in so-called natural SUSY models [32–36]. In such models, several of the SUSY particles are constrained to be light [35]: the top squarks, \tilde{t}_L and \tilde{t}_R , which have the same electroweak gauge couplings as the left- (L) and right- (R) handed top quarks, respectively; the bottom squark with L-handed couplings (\tilde{b}_L); the gluino (\tilde{g}); and the Higgsinos (\tilde{H}). In SUSY models that conserve R -parity—a multiplicative quantum number equal to $+1$ for SM particles and -1 for their SUSY partners [37, 38]—SUSY particles must be produced in pairs and each SUSY particle decay chain must terminate in the production of the lightest supersymmetric particle (LSP). The LSP is therefore stable and, if weakly interacting, can in principle account for some or all of the astrophysical dark matter [39–41].

Motivated by the naturalness-based expectations that both the gluino and the top squark should be relatively light, we search for gluino pair production with decays to either off- or on-mass-shell top squarks. Furthermore, gluino pair production has a large cross section relative to most other SUSY pair-production processes, for a fixed SUSY particle mass. Each gluino is assumed to decay via the process $\tilde{g} \rightarrow \tilde{t}_1 \bar{t}$ (or the conjugate final state), where the top squark mass eigenstate, \tilde{t}_1 , is the lighter of the two physical superpositions of \tilde{t}_L and \tilde{t}_R . Depending on the mass spectrum of the model, the top squark can be produced either on or off mass shell, and it is as-

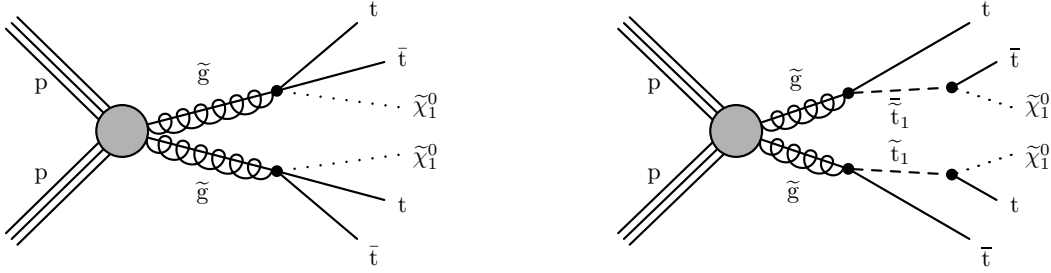


Figure 1: Gluino pair production and decay for the simplified models T1tttt (left) and T5tttt (right). In T1tttt, the gluino undergoes a three-body decay $\tilde{g} \rightarrow t\bar{t}\tilde{\chi}_1^0$ via a virtual intermediate top squark. In T5tttt, the gluino decays via the sequential two-body process $\tilde{g} \rightarrow \tilde{t}_1\bar{t}, \tilde{t}_1 \rightarrow t\tilde{\chi}_1^0$. Because gluinos are Majorana fermions, each one can decay to $\tilde{t}_1\bar{t}$ and to the charge conjugate final state \tilde{t}_1t . The filled circle represents the sum of processes that can lead to gluino pair production.

sumed to decay with 100% branching fraction via $\tilde{t}_1 \rightarrow t\tilde{\chi}_1^0$, where $\tilde{\chi}_1^0$ is a neutralino LSP. The neutralino is an electrically neutral mixture of the neutral Higgsinos and electroweak gauginos. Because the $\tilde{\chi}_1^0$ is weakly interacting, it would traverse the detector without depositing energy, much like a neutrino. As a consequence, neutralino production typically generates an apparent imbalance in the total transverse momentum of the event, \vec{p}_T^{miss} , which is a priori known to be essentially zero, apart from detector resolution effects and missing momentum carried by weakly interacting particles (e.g., neutrinos) or particles outside the detector acceptance.

Diagrams showing gluino pair production with decays to off-mass-shell and on-mass-shell top squarks are shown in Fig. 1 and are denoted as T1tttt and T5tttt, respectively, in the context of simplified models [42–45]. Such models, which include only a small subset of the full SUSY particle spectrum, are often used to quantify the results of searches, in spite of limitations in describing the potential complexities associated with a complete spectrum. The diagram for the T1tttt model does not explicitly show the off-mass-shell top squark, but the fundamental gluino decay vertex for both T1tttt and T5tttt models is the same. Thus, regardless of whether the top squark is produced on or off mass shell, each gluino ultimately decays via the process $\tilde{g} \rightarrow t\bar{t}\tilde{\chi}_1^0$, so signal events would contain a total of four top quarks and two neutralinos.

The final states for both T1tttt and T5tttt are characterized by a large number of jets, four of which are b jets from top quark decays. Depending on the decay modes of the accompanying W bosons, a range of lepton multiplicities is possible. We focus here on the single-lepton final state, where the lepton is either an electron or a muon, and a background estimation method specifically designed for this final state is a critical part of the analysis. Events from the extreme tails of the kinematic distributions for $t\bar{t}$ events can have properties that closely resemble those of signal events, including the presence of large p_T^{miss} generated by the neutrino from a leptonic W boson decay. Initial-state radiation (ISR) from strong interaction processes can enhance the jet multiplicity, producing another characteristic feature of signal events. Quantifying the effects of ISR is a critical element of the analysis.

The signature used here to search for the processes shown in Fig. 1 is characterized not only by the presence of an isolated high transverse momentum (p_T) lepton, multiple jets, at least one b-tagged jet, and large p_T^{miss} , but also by additional kinematic variables. The first of these is m_T , defined as the transverse mass of the system consisting of the lepton and the \vec{p}_T^{miss} in the event. Apart from resolution and small effects from off-mass-shell W boson production, m_T is bounded above by m_W for events with a single leptonically decaying W boson, and this

variable is effective in suppressing the otherwise dominant single-lepton $t\bar{t}$ background, as well as background from W +jets events.

Largely because of the effectiveness of the m_T variable in helping to suppress the single-lepton $t\bar{t}$ background, the residual background in the signal regions arises predominantly from a single SM process, dilepton $t\bar{t}$ production. In such background events, both W bosons from the $t \rightarrow bW$ decays produce leptons, but only one of the two leptons satisfies the lepton-identification criteria, as well as the requirements on the p_T , pseudorapidity (η), and isolation from other energetic particles in the event. This background includes $t\bar{t}$ events in which one or both of the W bosons decay into a τ lepton and its neutrino, provided that the subsequent τ decays produce a final state containing exactly one electron or muon satisfying the lepton selection requirements.

A second key kinematic variable, M_J , is defined as the scalar sum of the masses of large-radius jets in the event. This quantity is used both to characterize the mass scale of the event, providing discrimination between signal and background, and as a key part of the background estimation. A property of M_J exploited in this analysis is that, for $t\bar{t}$ events with large jet multiplicity, this variable is nearly uncorrelated with m_T . As a consequence, the M_J background shape at high m_T , which includes the signal region, can be measured to a very good approximation using the corresponding M_J shape in a low- m_T control sample. The quantity M_J was first discussed in phenomenological studies, for example, in Refs. [46–48]. Similar variables have been used by ATLAS for SUSY searches in all-hadronic final states using 8 TeV data [49, 50]. Studies of basic M_J properties and performance in CMS have been presented using early 13 TeV data [51].

Because the signal processes would populate regions of extreme tails of the SM distributions, it is important to determine the background in a manner that accounts for features of the detector behavior and of the SM backgrounds that may not be perfectly modeled in the simulated (Monte Carlo, MC) event samples. The background estimation method is constructed such that corrections derived from MC samples enter only at the level of double ratios of event yields, rather than as single ratios. This approach helps to control the impact of potential mismodeling on the background prediction because of the cancellation of many mismodeling effects. Systematic uncertainties in these predicted double ratios are obtained by performing tests using data control samples in regions that are kinematically similar but have only a very small potential contribution from signal events.

This paper is organized as follows. Sections 2 and 3 describe the simulated event samples and the CMS detector, respectively. Section 4 discusses the triggers used to collect the data, the event reconstruction methods, and the definitions of key quantities used in the analysis. The event selection and analysis regions are presented in Section 5, and the methodology used to predict the SM background is presented in Section 6. Section 7 summarizes the systematic uncertainties in the background predictions. Section 8 presents the event yields observed in the signal regions, the corresponding background predictions, the uncertainties associated with the signal efficiencies, and the resulting exclusion regions for the gluino pair-production models considered. Finally, the main results are summarized in Section 9.

2 Simulated event samples

The analysis makes use of several simulated event samples for modeling the signal and SM background processes. These samples are used in the overall design and optimization of the analysis procedures, in the determination of the efficiency for observing signal events, and in

the calculation of double-ratio correction factors, typically near unity, that are used in conjunction with event yields in control regions in data to estimate the backgrounds in the signal regions.

The production of $t\bar{t}$ +jets, W +jets, Z +jets, and quantum chromodynamics (QCD) multijet events is simulated with the MC generator MADGRAPH5_aMC@NLO 2.2.2 [52] in leading-order (LO) mode for 2016 samples and MADGRAPH5_aMC@NLO 2.4.2 for 2017 and 2018 samples. Single top quark events are modeled with MADGRAPH5_aMC@NLO at next-to-leading order (NLO) for the s -channel and with POWHEG v2 [53, 54] for the t -channel and for associated tW production. Additional small backgrounds, such as $t\bar{t}$ production in association with bosons, diboson processes, and $t\bar{t}t\bar{t}$, are similarly produced at NLO with either MADGRAPH5_aMC@NLO or POWHEG. The events are generated using the NNPDF 2.3 [55] set of parton distribution functions (PDF) for 2016 samples and the NNPDF 3.1 [56] PDF set for 2017 and 2018 samples. Parton showering and fragmentation are performed with the PYTHIA 8.2 [57] generator using the CUETP8M1 [58] underlying event model for the 2016 samples and the CP5 [59] model for the 2017 and 2018 samples. The detector simulation is performed with GEANT4 [60]. The cross sections used to scale simulated event yields are based on the highest order calculation available.

Signal events for the T1tttt and T5tttt simplified SUSY models are generated in a manner similar to that for the SM backgrounds, with the MADGRAPH5_aMC@NLO 2.4.2 generator in LO mode using the NNPDF 2.3 PDF set for 2016 samples and the NNPDF 3.1 PDF set for the 2017 and 2018 samples. Parton showering and fragmentation are performed with the PYTHIA 8.2 generator using the CUETP8M1 [58] underlying event model for the 2016 samples and the CP2 [59] model for the 2017 and 2018 samples. However, because of the large number of model scenarios that must be considered, the detector simulation is performed with the CMS fast simulation package [61, 62], with scale factors applied to account for differences with respect to the full simulation. Event samples are generated for a representative set of model scenarios by scanning over the relevant mass ranges for the \tilde{g} and $\tilde{\chi}_1^0$, and the yields are normalized to the cross-section at approximate next-to-NLO, including next-to-next-to-leading-logarithmic (NNLL) contributions [63–71]. The modeling of the event kinematics is further improved by reweighting the distribution of the number of ISR jets to match the data based on a measurement in a dilepton $t\bar{t}$ sample with two b -tagged jets [72].

Throughout this paper, two T1tttt benchmark models are used to illustrate typical signal behavior. The T1tttt(2100,100) model, with masses $m(\tilde{g}) = 2100$ GeV and $m(\tilde{\chi}_1^0) = 100$ GeV, corresponds to a scenario with a large mass splitting between the gluino and the neutralino. This mass combination probes the sensitivity of the analysis to a low cross section (0.59 fb) process that has a hard p_T^{miss} distribution, which results in a relatively high signal efficiency. The T1tttt(1900,1250) model, with masses $m(\tilde{g}) = 1900$ GeV and $m(\tilde{\chi}_1^0) = 1250$ GeV, corresponds to a scenario with a relatively small mass splitting (referred to as a compressed spectrum) between the gluino and the neutralino. Here the cross section is higher (1.6 fb) because the gluino mass is lower than for the T1tttt(2100,100) model, but the sensitivity suffers from a low signal efficiency due to the soft p_T^{miss} distribution.

Finally, to model the presence of additional pp collisions from the same or adjacent bunch crossing as the primary hard scattering process (pileup interactions), the simulated events are overlaid with multiple minimum bias events (generated with the PYTHIA 8.2 generator), such that the minimum bias event multiplicity in simulation matches that observed in data.

3 CMS detector

The central feature of the CMS detector is a superconducting solenoid of 6 m internal diameter, providing a magnetic field of 3.8 T. Within the solenoid volume are a silicon pixel and strip tracker, a lead tungstate crystal electromagnetic calorimeter, and a brass and scintillator hadron calorimeter. Each of these systems is composed of a barrel and two endcap sections. The tracking detectors cover the pseudorapidity range $|\eta| < 2.5$. For the electromagnetic and hadronic calorimeters, the barrel and endcap detectors together cover the range $|\eta| < 3.0$. Forward calorimeters extend the coverage to $3.0 < |\eta| < 5.0$. Muons are measured and identified in both barrel and endcap systems, which together cover the pseudorapidity range $|\eta| < 2.4$. The detection planes are based on three technologies: drift tubes, cathode strip chambers, and resistive plate chambers, which are embedded in the steel flux-return yoke outside the solenoid. The detector is nearly hermetic, permitting accurate measurements of \vec{p}_T^{miss} . Events of interest are selected using a two-tiered trigger system [73]. The first level (L1), composed of custom hardware processors, uses information from the calorimeters and muon detectors to select events at a rate of around 100 kHz within a time interval of less than $4 \mu\text{s}$. The second level, known as the high-level trigger, consists of a farm of processors running a version of the full event reconstruction software optimized for fast processing, and reduces the event rate to around 1 kHz before data storage. A more detailed description of the CMS detector, together with a definition of the coordinate system used and the relevant kinematic variables, can be found in Ref. [74].

4 Trigger requirements and event reconstruction

The data sample used in this analysis was obtained with the logical OR of event triggers that require either missing transverse momentum larger than 100–120 GeV, or a single lepton with p_T greater than 24–32 GeV, or a single lepton with $p_T > 15$ GeV accompanied by transverse hadronic energy greater than 350–400 GeV, where the exact thresholds depended on the instantaneous luminosity. The triggers based on missing transverse momentum quantities alone, without a lepton requirement, have high asymptotic efficiency (about 99%), but they only reach the efficiency plateau for p_T^{miss} larger than 250–300 GeV. The single-lepton triggers are therefore included to ensure high efficiency at lower values of p_T^{miss} , and they bring the analysis trigger efficiency up to nearly 100% for $p_T^{\text{miss}} > 200$ GeV.

The total trigger efficiency has been studied as a function of the analysis variables N_{jets} , N_{b} , M_J , and m_T , defined later in this section, in the region with $p_T^{\text{miss}} > 200$ GeV. The efficiency is close to 100% and is found to be uniform with respect to these analysis variables over the three years of data taking. The systematic uncertainty in the trigger efficiency is estimated to be 0.5%.

Event reconstruction proceeds from particles identified by the particle-flow (PF) algorithm [75], which uses information from the tracker, calorimeters, and muon systems to identify PF candidates as electrons, muons, charged or neutral hadrons, or photons. Charged-particle tracks are required to originate from the event primary pp interaction vertex, defined as the candidate vertex with the largest value of summed physics-object p_T^2 . The physics objects used in this calculation are the jets, clustered using the anti- k_T jet finding algorithm [76, 77] with the tracks assigned to candidate vertices as inputs, and the associated missing transverse momentum, taken as the negative vector sum of the p_T of those jets.

Electrons are reconstructed by associating a charged-particle track with electromagnetic calorimeter superclusters [78]. The resulting electron candidates are required to have $p_T > 20$ GeV and $|\eta| < 2.5$, and to satisfy identification criteria designed to reject light-parton jets, photon

conversions, and electrons produced in the decays of heavy-flavor hadrons. Muons are reconstructed by associating tracks in the muon system with those found in the silicon tracker [79]. Muon candidates are required to satisfy $p_T > 20$ GeV and $|\eta| < 2.4$.

To preferentially select leptons that originate in the decay of W bosons, and to suppress backgrounds in which the leptons are produced in the decays of hadrons containing heavy quarks, leptons are required to be isolated from other PF candidates. Isolation is quantified using an optimized version of the “mini-isolation” variable originally suggested in Ref. [80]. The isolation I_{mini} is calculated by summing the transverse momentum of the charged hadrons, neutral hadrons, and photons within $\Delta R \equiv \sqrt{(\Delta\phi)^2 + (\Delta\eta)^2} < R_0$ of the lepton momentum vector \vec{p}_T^ℓ , where ϕ is the azimuthal angle in radians and R_0 is given by 0.2 for $p_T^\ell \leq 50$ GeV, $(10 \text{ GeV})/p_T^\ell$ for $50 < p_T^\ell < 200$ GeV, and 0.05 for $p_T^\ell \geq 200$ GeV. Electrons (muons) are then required to satisfy $I_{\text{mini}}/p_T^\ell < 0.1$ (0.2).

Jets are reconstructed by clustering charged and neutral PF candidates using the anti- k_T algorithm [76] with a distance parameter of $R = 0.4$, as implemented in the FASTJET package [77]. Jets are corrected using a p_T - and η -dependent jet energy calibration [81], and the estimated energy contribution to the jet p_T from pileup [82] is subtracted. Jets are then required to satisfy $p_T > 30$ GeV and $|\eta| < 2.4$, as well as jet identification criteria [81]. Finally, jets that have PF constituents matched to an isolated lepton are removed from the jet collection. The number of jets satisfying these requirements is a key quantity in the analysis and is denoted N_{jets} .

Jets are “tagged” as originating from the hadronization of b quarks using the deep combined secondary vertex (DeepCSV) algorithm [83]. For the medium working point chosen here, the signal efficiency for identifying b jets with $p_T > 30$ GeV in $t\bar{t}$ events is about 68%. The probability to misidentify jets in $t\bar{t}$ events arising from c quarks is approximately 12%, while the probability to misidentify jets associated with light-flavor quarks or gluons as b jets is approximately 1%. The number of b-tagged jets is another key quantity in the analysis and is denoted N_b .

The analysis also makes use of large-radius (large- R) jets, denoted generically with the symbol J . These jets are constructed by clustering the standard small- R ($R = 0.4$) jets described above, as well as isolated leptons, into large- R ($R = 1.4$) jets using the anti- k_T algorithm. Starting the clustering from small- R jets takes advantage of the corrections that are applied to these jets. The masses, $m(J_i)$, of the individual large- R jets reflect the p_T spectrum and multiplicity of the clustered objects, as well as their angular spread. By summing the masses of all large- R jets in an event, we obtain the variable M_J , which is central to the analysis method:

$$M_J = \sum_{J_i=\text{large-}R \text{ jets}} m(J_i). \quad (1)$$

For $t\bar{t}$ events with a small contribution from ISR, the distribution of M_J has an approximate cutoff at $2m_t$ [17]. Thus, in the absence of ISR, the requirement $M_J > 2m_t$ is expected to remove most of the $t\bar{t}$ background. In contrast, the M_J distribution for signal events typically extends to larger values of M_J because of the presence of more than two top quarks in the decay chain. However, as discussed in Refs. [17, 19], the presence of a significant amount of ISR in a subset of $t\bar{t}$ background events generates a tail at large values of M_J , and understanding this effect is critical for estimating the remaining background in the analysis.

The missing transverse momentum, \vec{p}_T^{miss} , is defined as the negative vector sum of the transverse momenta of all PF candidates and is calibrated taking into account the jet energy corrections. Dedicated event filters designed to reject instrumental noise are applied to further improve the correspondence between the reconstructed and the genuine p_T^{miss} [84, 85].

To suppress backgrounds characterized by the presence of a single W boson decaying leptonically, and without any other significant source of \vec{p}_T^{miss} apart from the neutrino from this process, we use the quantity m_T , defined as the transverse mass of the system consisting of the lepton and the missing transverse momentum vector,

$$m_T = \sqrt{2p_T^\ell p_T^{\text{miss}} [1 - \cos(\Delta\phi_{\ell, \vec{p}_T^{\text{miss}}})]}, \quad (2)$$

where $\Delta\phi_{\ell, \vec{p}_T^{\text{miss}}}$ is the difference between the azimuthal angles of \vec{p}_T^ℓ and \vec{p}_T^{miss} . For both $t\bar{t}$ events with a single leptonic W decay, and for W+jets events with leptonic W boson decay, the m_T distribution peaks strongly below the W boson mass.

Although the event selection requires exactly one identified isolated lepton, backgrounds can still arise from processes in which two leptons are produced but only one satisfies the identification and isolation criteria. The dominant contribution to this type of background arises from $t\bar{t}$ events with two leptonic W boson decays, including W decays involving τ leptons, which can themselves decay into hadrons, electrons, or muons. To help suppress such dilepton backgrounds, events are vetoed that contain a broader category of candidates for the second lepton, referred to as veto tracks, which do not satisfy the stringent lepton identification requirements. These include two categories of charged-particle tracks: isolated leptons satisfying looser identification criteria than lepton candidates, as well as a relaxed momentum requirement, $p_T > 10 \text{ GeV}$, and isolated charged-hadron PF candidates, which must satisfy $p_T > 15 \text{ GeV}$. For example, isolated charged hadrons can arise in τ decays. For either category, the charge of the veto track must be opposite to that of the identified lepton candidate in the event. To maintain a high selection efficiency for signal events, lepton veto tracks must also satisfy a requirement on the quantity m_{T2} [86, 87],

$$m_{T2}(\ell, v, \vec{p}_T^{\text{miss}}) = \min_{\vec{p}_1 + \vec{p}_2 = \vec{p}_T^{\text{miss}}} \left[\max \{ m_T(\vec{p}_\ell, \vec{p}_1), m_T(\vec{p}_v, \vec{p}_2) \} \right], \quad (3)$$

where v refers to the veto track. The minimization is taken over all possible pairs of momenta \vec{p}_1 and \vec{p}_2 that sum to the \vec{p}_T^{miss} . For the dominant background, $t\bar{t}$, if the lepton, the veto track, and the missing transverse momentum all result from a pair of leptonically decaying W bosons, m_{T2} is bounded above by the W boson mass. We improve the signal efficiency by requiring $m_{T2} < 80 \text{ GeV}$ for loosely identified leptonic tracks and $m_{T2} < 60 \text{ GeV}$ for hadronic tracks.

Finally, we define S_T as the scalar sum of the transverse momenta of all the small-R jets and all leptons passing the selection.

5 Event selection and analysis regions

Using the quantities and criteria defined in Section 4, events are selected that have exactly one isolated charged lepton (an electron or a muon), no veto tracks, $M_J > 250 \text{ GeV}$, $S_T > 500 \text{ GeV}$, $p_T^{\text{miss}} > 200 \text{ GeV}$, and at least seven (six) small-R jets if $p_T^{\text{miss}} \leq 500 \text{ GeV}$ ($p_T^{\text{miss}} > 500 \text{ GeV}$). At least one of the jets must be tagged as originating from a bottom quark. After this set of requirements, referred to in the following as the *baseline selection*, more than 85% of the remaining SM background arises from $t\bar{t}$ production. The contributions from events with a single top quark or a W boson in association with jets are each about 4–5%, while the combined contribution from $t\bar{t}W$ and $t\bar{t}Z$ events is about 2%. The background from QCD multijet events after the baseline selection is very small. Approximately 40% of signal T1tttt events are selected with the single-lepton requirement only.

To improve the sensitivity to the signal and to provide a method for the background estimation, the events satisfying the baseline selection are divided into a set of signal and control regions in the M_J - m_T plane and in bins of p_T^{miss} , N_{jets} , and N_b . In each of the three p_T^{miss} regions, $200 < p_T^{\text{miss}} \leq 350$ GeV, $350 < p_T^{\text{miss}} \leq 500$ GeV, and $p_T^{\text{miss}} > 500$ GeV, the M_J - m_T plane is divided into six regions, referred to as R1, R2A, R2B, R3, R4A, and R4B, as shown in Fig. 2. The signal regions are R4A and R4B, while R1, R2A, R2B, and R3 serve as control regions. Potential signal contamination in the control regions is taken into account using a fit method described in Section 6. Regions denoted with the letter A are referred to as low M_J , while regions denoted with the letter B are referred to as high M_J . The control regions R1, R2A, and R3 are used to estimate the background in signal region R4A, while the control regions R1, R2B, and R3 are used to estimate the background in signal region R4B. (In discussions where the distinction between R2A and R2B, or between R4A and R4B, is irrelevant, we refer to these regions generically as R2 and R4.) As seen in Fig. 2, for each of the three regions in p_T^{miss} , the M_J ranges for R2A and R4A (low M_J) and for R2B and R4B (high M_J) are

- $200 < p_T^{\text{miss}} \leq 350$ GeV: $400 < M_J \leq 500$ GeV (low M_J) and $M_J > 500$ GeV (high M_J)
- $350 < p_T^{\text{miss}} \leq 500$ GeV: $450 < M_J \leq 650$ GeV (low M_J) and $M_J > 650$ GeV (high M_J)
- $p_T^{\text{miss}} > 500$ GeV: $500 < M_J \leq 800$ GeV (low M_J) and $M_J > 800$ GeV (high M_J).

The use of six regions in the M_J - m_T plane (in each bin of p_T^{miss}) is an improvement over the original method used in Refs. [17, 19], where only four regions were used: R1, R2 (combining R2A and R2B), R3, and R4 (combining R4A and R4B). The larger event yields in the full Run 2 data sample allow for this additional division of the M_J - m_T plane. By separating each of the original ‘‘high’’ M_J regions into two bins, we are able to obtain additional sensitivity to SUSY models with large mass splittings, which tend to populate the highest M_J regions with a significant number of events. In addition, the values of M_J corresponding to the boundaries between these regions increase with p_T^{miss} , improving the expected precision in the background prediction.

Regions R2A, R2B, R4A, and R4B are further subdivided into bins of N_{jets} and N_b to increase sensitivity to the signal:

- two N_{jets} bins: $N_{\text{jets}} = 7$ ($6 \leq N_{\text{jets}} \leq 7$) for $p_T^{\text{miss}} \leq 500$ GeV ($p_T^{\text{miss}} > 500$ GeV) and $N_{\text{jets}} \geq 8$
- three N_b bins: $N_b = 1$, $N_b = 2$, and $N_b \geq 3$.

The total number of signal regions is therefore $3(p_T^{\text{miss}}) \times 2(M_J) \times 2(N_{\text{jets}}) \times 3(N_b) = 36$. Given that the main background processes have two or fewer b quarks, the total SM contribution to the $N_b \geq 3$ bins is very small and is driven by the b jet mistag rate. Signal events in the T1tttt model are expected to populate primarily the bins with $N_b \geq 2$, while bins with $N_b = 1$ mainly serve to test the method in a background dominated region.

Because of the common use of R1 and R3 in the background estimations for R4A and R4B, as well as the integration over N_{jets} and N_b in the R1 and R3 regions, there are statistical correlations between the background predictions, which are taken into account in the fitting methodology (Section 6).

6 Background estimation method

The method for estimating the background yields in each of the signal bins takes advantage of the fact that the M_J and m_T distributions of background events with a significant amount

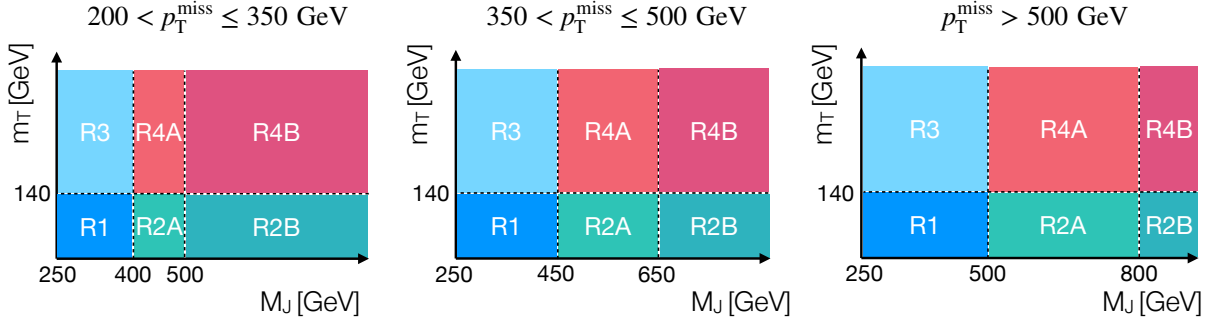


Figure 2: Analysis regions defined for each bin in p_T^{miss} . For the signal models considered here, the regions R1, R2A, R2B, and R3 are dominated by background, while R4A and R4B would have a significant signal contribution. In the combined fit performed to the event yields observed in these regions, signal contributions are allowed in the background-dominated regions. The R2A, R2B, R4A, and R4B regions are further divided into bins of N_{jets} and N_{b} , as discussed in the text.

of ISR are largely uncorrelated and that there are background-dominated control samples that can be used to test the method and establish systematic uncertainties. Figure 3 shows the two-dimensional distribution of simulated $t\bar{t}$ events in the variables M_J and m_T , with single-lepton and dilepton events shown with separate symbols. The three background-dominated regions (R1, R2, and R3) and the signal region (R4) are indicated. (For simplicity, the separate A and B regions for R2 and R4 are not shown in this figure.) The low- m_T region, $m_T \leq 140$ GeV, is dominated by $t\bar{t}$ single-lepton events, and the rapid falloff in the number of such events as m_T increases is apparent. In contrast, the high- m_T region, $m_T > 140$ GeV, is dominated by $t\bar{t}$ dilepton events. As discussed in Refs. [17, 19], the M_J distributions for the events in these two regions become nearly identical in the presence of significant ISR, which is enforced by the jet multiplicity requirements. This behavior allows us to measure the shape of the M_J distribution at low m_T with good statistical precision and then use it to obtain a background prediction in the high- m_T region by normalizing it to the event yield in R3.

To estimate the background contribution in each of the signal bins, a modified version of an “ABCD” method is used. Here, the symbols A, B, C, and D refer to four regions in a two-dimensional space in the data, where one of the regions is dominated by signal and the other three are dominated by backgrounds. In a standard ABCD method, the background rate ($\mu_{\text{region}}^{\text{bkg}}$) in the signal region (in this case, either R4A or R4B) is estimated from the yields (N_{region}) in three control regions using

$$\begin{aligned}\mu_{\text{R4A}}^{\text{bkg}} &= \frac{N_{\text{R2A}} N_{\text{R3}}}{N_{\text{R1}}}, \\ \mu_{\text{R4B}}^{\text{bkg}} &= \frac{N_{\text{R2B}} N_{\text{R3}}}{N_{\text{R1}}},\end{aligned}\tag{4}$$

where the labels of the regions correspond to those shown in Fig. 2. The background prediction is unbiased in the limit that the two variables that define the plane (in this case, M_J and m_T) are uncorrelated. The effect of any residual correlation can be taken into account by multiplying these background predictions by correction factors κ_A and κ_B ,

$$\begin{aligned}\mu_{\text{R4A}}^{\text{bkg}} &= \kappa_A \left(\frac{N_{\text{R2A}} N_{\text{R3}}}{N_{\text{R1}}} \right), \\ \mu_{\text{R4B}}^{\text{bkg}} &= \kappa_B \left(\frac{N_{\text{R2B}} N_{\text{R3}}}{N_{\text{R1}}} \right),\end{aligned}\tag{5}$$

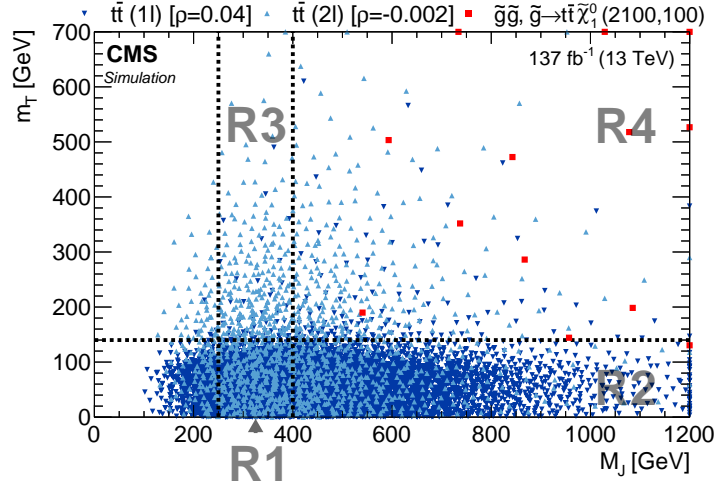


Figure 3: Distribution of simulated single-lepton $t\bar{t}$ events (dark-blue inverted triangles) and dilepton $t\bar{t}$ events (light-blue triangles) in the M_J - m_T plane after applying the baseline selection and requiring at least two b jets. A representative random sample of T1ttt events with $m(\tilde{g}) = 2100$ GeV and $m(\tilde{\chi}_1^0) = 100$ GeV is also shown for comparison (red squares). Each marker represents one expected event in the full data sample. Overflow events are placed on the edges of the plot. The values of the correlation coefficients ρ for each of the background processes are given in the legend. Region R4, which is further split into smaller bins R4A and R4B, is the nominal signal region, while R1, R2, and R3 serve as control regions. This plot is only illustrative, because the boundary between R1 and R2, as well as between R3 and R4, is p_T^{miss} -dependent. The line shown at 400 GeV corresponds to the value used for the lowest p_T^{miss} bin. Additional sensitivity is obtained by binning the events in p_T^{miss} , N_{jets} , and N_b .

which are double ratios obtained from simulated event samples:

$$\begin{aligned}\kappa_A &= \frac{N_{R4A}^{\text{MC,bkg}} / N_{R3}^{\text{MC,bkg}}}{N_{R2A}^{\text{MC,bkg}} / N_{R1}^{\text{MC,bkg}}} \\ \kappa_B &= \frac{N_{R4B}^{\text{MC,bkg}} / N_{R3}^{\text{MC,bkg}}}{N_{R2B}^{\text{MC,bkg}} / N_{R1}^{\text{MC,bkg}}}\end{aligned}\quad (6)$$

When the two ABCD variables are uncorrelated, or nearly so, the κ factors are close to unity. This procedure ignores potential signal contamination in the control regions, which is accounted for by incorporating the methods described above into a fit that includes both signal and background components.

In principle, this calculation to estimate the background can be performed for each of the 36 signal bins by applying this procedure in 36 independent ABCD planes. However, such an approach would incur large statistical uncertainties in some bins due to the small number of events in R3 regions. This problem is especially important in bins with a large number of jets, where the M_J distribution shifts to higher values and the number of background events expected in R4 can even exceed the background in R3.

To alleviate this problem, we exploit the fact that, after the baseline selection, the background is dominated by a single source ($t\bar{t}$ events), and the shapes of the N_{jets} distributions are nearly identical for the single-lepton and dilepton components, because of the large amount of ISR. As a result, the m_T distribution is approximately independent of N_{jets} and N_b . More specifically, we find that for M_J values corresponding to the R1 and R3 regions, the ratios of high- m_T to low-

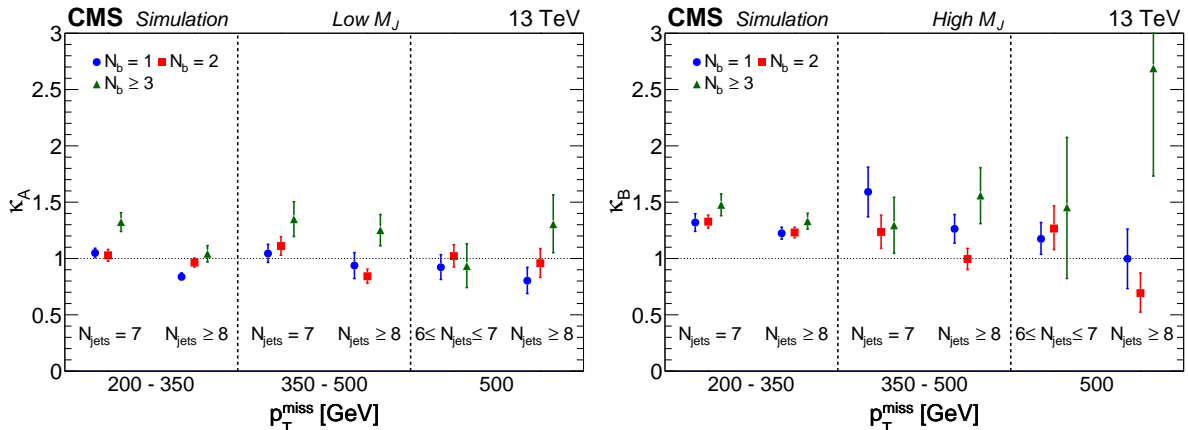


Figure 4: Values of the double-ratio κ for each of the 18 signal bins of the low- M_J ABCD planes, i.e., R1-R2A-R3-R4A (left), and the 18 signal bins of the high- M_J ABCD planes, i.e., R1-R2B-R3-R4B (right), calculated using the simulated SM background. The κ factors are close to unity, indicating a small correlation between M_J and m_T . The uncertainties shown are statistical only.

m_T event yields do not vary substantially between events with seven or more jets, and across N_b within these N_{jets} bins. We exploit this result by integrating the event yields in the low- M_J regions (R1 and R3) over the N_{jets} and N_b bins for each p_T^{miss} bin. This procedure increases the statistical power of the ABCD method but also introduces a correlation among the predictions from Eq. (5) for the N_{jets} and N_b bins associated with a given p_T^{miss} bin.

Figure 4 shows the values of the κ factors obtained from simulation (computed after integrating over N_{jets} and N_b in R1 and R3 only) for the 18 signal bins of the low- M_J ABCD planes, i.e., R1-R2A-R3-R4A (left plot), and the 18 signal bins of the high- M_J ABCD planes, i.e., R1-R2B-R3-R4B (right plot). These values are close to unity for the low- M_J regions and are slightly above unity for the high- M_J regions. The deviation from unity is due to the presence of mismeasured jets in single-lepton $t\bar{t}$ events, which produces a correlation between m_T and M_J . The additional p_T^{miss} arising from the jet mismeasurement allows these events to migrate from the low- m_T to the high- m_T region. Since the mismeasured p_T^{miss} is correlated with hadronic activity, these events typically also have larger M_J values relative to well-reconstructed events. Consequently, their presence at high m_T results in a difference between the shapes of the M_J distributions for low- m_T and high- m_T events and thus results in a κ value larger than unity. In addition to the statistical uncertainties shown in Fig. 4, systematic uncertainties are obtained from studies of the modeling of the κ values in dedicated data control samples, including both a sample with high purity of dilepton $t\bar{t}$ events as well as a sample enriched in mismeasured single-lepton $t\bar{t}$ events, as discussed in Section 7.

The method described above is implemented with a maximum likelihood fit to the event yields observed in data using a likelihood function that incorporates both the statistical and systematic uncertainties in κ_A and κ_B . The fit also takes into account the correlations associated with the common R1 and R3 yields that arise from the integration over N_{jets} and N_b , and it accounts for the signal contamination in the control regions.

The signal strength is the only parameter that enters the likelihood in a way that extends across p_T^{miss} bins. We can therefore define the correlation model within each p_T^{miss} bin and then take the product over p_T^{miss} bins to construct the full likelihood function. Let $\mu_{i,j,k}^{\text{bkg}}$ be the estimated (Poisson) mean background in each region, where i indicates the p_T^{miss} bin, $j \in S$ with $S \equiv \{\text{R1},$

R2A, R2B, R3, R4A, R4B}, and k runs over the six $N_{\text{jets}}-N_b$ bins. Then, in a given p_T^{miss} bin, the 26 background rates (one each for R1 and R3 and six each for R2A, R2B, R4A, and R4B) can be expressed in terms of 14 floating fit parameters θ (one each for R1 and R3 and six each for R2A and R2B) and the 12 correction factors κ (κ_A and κ_B for each of the six N_{jets} and N_b bins for a fixed p_T^{miss} bin) as

$$\begin{aligned}\mu_{R1}^{\text{bkg}} &= \theta_{R1}, & \mu_{R2A,k}^{\text{bkg}} &= \theta_{R2A,k}, \\ & & \mu_{R2B,k}^{\text{bkg}} &= \theta_{R2B,k}, \\ \mu_{R3}^{\text{bkg}} &= \theta_{R3}, & \mu_{R4A,k}^{\text{bkg}} &= \kappa_{A,k} \theta_{R2A,k} (\theta_{R3}/\theta_{R1}), \\ & & \mu_{R4B,k}^{\text{bkg}} &= \kappa_{B,k} \theta_{R2B,k} (\theta_{R3}/\theta_{R1}).\end{aligned}\tag{7}$$

Here, the i index for the three p_T^{miss} bins is suppressed, because it applies identically to all parameters in the equations. In addition, the k index over the N_{jets} and N_b bins is omitted for terms that are integrated over these quantities, i.e., for the parameters for the R1 and R3 regions. The quantity θ_{R3}/θ_{R1} is simply the ratio between the background event rates in regions R3 and R1, summed over N_{jets} and N_b . To obtain the prediction for the mean background, this ratio is then multiplied by the appropriate rate $\theta_{R2A,k}$ or $\theta_{R2B,k}$ and then corrected with the appropriate value κ_A or κ_B for the given bin in N_{jets} and N_b .

Defining $N_{i,j,k}^{\text{data}}$ as the observed data yield in each region and bin, $\mu_{i,j,k}^{\text{MC,sig}}$ as the corresponding expected signal rate, and r as the parameter quantifying the signal strength relative to the expected yield across all analysis regions, we can write the likelihood function as

$$\begin{aligned}\mathcal{L} &= \prod_i^{p_T^{\text{miss}} \text{bins}} \mathcal{L}_{\text{ABCD},i}^{\text{data}} \mathcal{L}_{\text{sig},i}^{\text{MC}}, \\ \mathcal{L}_{\text{ABCD},i}^{\text{data}} &= \prod_{j \in S} \prod_{k=1}^{N_{\text{bins}}(j)} \text{Poisson}(N_{i,j,k}^{\text{data}} | \mu_{i,j,k}^{\text{bkg}} + r \mu_{i,j,k}^{\text{MC,sig}}), \\ \mathcal{L}_{\text{sig},i}^{\text{MC}} &= \prod_{j \in S} \prod_{k=1}^{N_{\text{bins}}(j)} \text{Poisson}(N_{i,j,k}^{\text{MC,sig}} | \mu_{i,j,k}^{\text{MC,sig}}).\end{aligned}\tag{8}$$

Given the integration over N_{jets} and N_b in R1 and R3, $N_{\text{bins}}(\text{R1}) = N_{\text{bins}}(\text{R3}) = 1$, while $N_{\text{bins}}(\text{R2A}) = N_{\text{bins}}(\text{R2B}) = N_{\text{bins}}(\text{R4A}) = N_{\text{bins}}(\text{R4B}) = 6$.

In Eq. (8), the $\mathcal{L}_{\text{ABCD},i}^{\text{data}}$ terms account for the statistical uncertainty in the observed data yield in each bin, and the $\mathcal{L}_{\text{sig},i}^{\text{MC}}$ terms account for the uncertainty in the signal shape, due to the finite size of the MC samples. The statistical uncertainties in the κ factors due to the finite size of the simulated background event samples are implemented as Gaussian constraints. The signal systematic uncertainties are incorporated in the likelihood function as log-normal constraints with a nuisance parameter for each uncorrelated source of uncertainty. These terms are not explicitly shown in the likelihood function above for simplicity.

The likelihood function defined in Eq. (8) is employed in two separate types of fits that provide complementary but compatible background estimates based on an ABCD model. The ‘‘R1–R3 fit’’ is used to test the agreement between the observed event yields (R4) and the predictions (based on R1, R2, and R3 event yields) under the null (i.e., the background-only) hypothesis. In this approach, we exclude the observations in the signal regions in the likelihood and fix the signal strength r to 0. This procedure involves as many unknowns as constraints. As a result, the estimated background rates in regions R1, R2, and R3 become simply the observed values in

those bins, and we obtain predictions for the signal regions that do not depend on the observed N_{R4}^{data} . The R1–R3 fit thus corresponds to the standard ABCD method with κ corrections, and the likelihood machinery becomes just a convenient way to solve the system of equations and propagate the various uncertainties.

In contrast, the “R1–R4 fit” also makes use of the observations in the signal regions, and it can therefore provide an estimate of the signal strength r , while also allowing for signal events to populate the control regions. We also use the R1–R4 fit with the constraint $r = 0$ to assess the agreement between the data and the background predictions in the null hypothesis.

7 Background systematic uncertainties

The background estimation procedure described in Section 6 relies on the approximate independence of the kinematic variables M_J and m_T , as well as on the ability of the simulation to correctly model any residual correlation, which would manifest as a departure of κ from unity. The approximate independence of M_J and m_T is a consequence of two key features of the data, namely, that the high- m_T sample is composed primarily of dilepton $t\bar{t}$ events and that the M_J spectra of $t\bar{t}$ events with one and two leptons become highly similar in the presence of ISR jets. A residual correlation of M_J and m_T can arise either from (i) contributions to the overall M_J shape from backgrounds other than single-lepton $t\bar{t}$ at low m_T and dilepton $t\bar{t}$ at high m_T or from (ii) subleading kinematic effects that result in the gradual divergence of the single-lepton and dilepton M_J shapes as a function of the analysis binning variables. As an example of (i), simulation studies show that the deviation of κ from unity for the high- M_J ABCD planes, most pronounced at low p_T^{miss} , can arise from mismeasured single-lepton $t\bar{t}$ events that populate the high- m_T region. A classification and study of such mechanisms was presented in Ref. [17]. Based on this understanding, the systematic uncertainties in the background estimate are obtained by quantifying the ability of the simulation to predict the behavior of κ in control samples in data with varying background composition and as a function of the analysis binning variables.

7.1 Control sample strategy

Two control samples are used to assess the ability of the simulation to reproduce the behavior of κ in the data: a 2ℓ sample composed of events with two reconstructed leptons and a 1ℓ , 5–6 jet sample composed of events with a single reconstructed lepton and either five or six jets.

Because it is composed primarily of $t\bar{t}$ dilepton events, the 2ℓ control sample allows us to assess the validity of the main assertion of the analysis, namely that the shapes of the M_J distributions for 1ℓ and 2ℓ $t\bar{t}$ events approximately converge at high jet multiplicities. The MC predictions for κ are tested independently as a function of N_{jets} and p_T^{miss} using this control sample, because simulation studies show no significant correlation in the κ behavior as a function of these two variables. The dilepton control sample is not used to probe the modeling of κ as a function of N_b , which is instead studied in the 5–6 jet control sample described below. Events in the dilepton control sample with $N_b \geq 2$ are excluded to avoid potential signal contamination.

Except for the case of the dilepton $t\bar{t}$ process, it is not possible to find useful control samples where a particular background category dominates. As a consequence, we cannot completely factorize the uncertainty in κ arising from mismodeling of the background composition and from mismodeling the m_T - M_J correlation for a particular background. However, we are able to define a control sample in which the background composition and kinematic characteristics are very similar to those in the signal regions, but in which the expected signal contribution

is too small to significantly affect the data vs. simulation comparison. The single-lepton, 5–6 jet sample satisfies these requirements. Both the κ values for individual background categories and the composition of background processes are very similar to those for events with $N_{\text{jets}} \geq 7$. We therefore use this control sample to quantify mismodeling of κ arising either from detector mismeasurement effects (which can result in a larger fraction of single-lepton $t\bar{t}$ events at high m_T), or from mismodeling of the background composition. An N_b -dependent uncertainty is derived from the lowest p_T^{miss} region (which is binned in N_b). Based on studies in simulation, any N_b dependence is not correlated with p_T^{miss} within the statistical precision of the sample, and therefore the uncertainties derived in the low- p_T^{miss} region can be used for all p_T^{miss} bins. Since the low- p_T^{miss} bin has the highest contribution from events with p_T^{miss} mismeasurement, this uncertainty also provides an estimate of the uncertainty in the modeling of κ in the presence of mismeasurement that is valid over the full p_T^{miss} range. We have verified in simulation that artificially increasing the fraction of mismeasured events has a consistent effect across the bins in the single-lepton, 5–6 jet control sample and the corresponding signal bins, so this effect would be detected in a study of this control sample.

7.2 Dilepton control sample results

We construct an alternate ABCD plane in which the high- m_T regions R3 and R4A/B are replaced with regions D3 and D4A/B, which are defined as having either two reconstructed leptons or one lepton and one isolated track. The new regions D3 and D4A/B are constructed to mimic the selection for R3 and R4A/B, respectively. For the events with two reconstructed leptons in D3 and D4A/B, the selection is modified as follows: the N_{jets} bin boundaries are lowered by 1 to keep the number of large- R jet constituents the same as in the single-lepton samples; the m_T requirement is not applied; and events with both $N_b = 0, 1$ are included to increase the size of the event sample. The lepton-plus-track events in D3 and D4A/B are required to pass the same selection as those in R3 and R4 except for the track veto. With these requirements, the sample is estimated from simulation to consist of between 75–85% $t\bar{t}$ dilepton events, depending on the p_T^{miss} and N_{jets} bin.

Using the dilepton control sample, we compute the values of κ in both simulation and data in the two N_{jets} bins at low p_T^{miss} , and integrated over N_{jets} in the intermediate- and high- p_T^{miss} bins. Figure 5 compares the κ values obtained from simulation with those observed in data in the dilepton control sample. We observe that these values are consistent within the total statistical uncertainties, and we therefore assign the statistical uncertainty in this comparison as the systematic uncertainty in κ as follows. We take the uncertainty associated with the N_{jets} dependence of κ from the lowest p_T^{miss} bin, specifically, 8 (8)% for low N_{jets} and 9 (8)% for high N_{jets} at low M_J (high M_J), and use these values in the intermediate- and high- p_T^{miss} bins as well. This procedure is based on the observation that in simulated event samples the dependence of κ on N_{jets} is consistent across p_T^{miss} bins. This uncertainty also accounts for potential mismodeling of κ at low p_T^{miss} . Then, to account for additional possible sources of mismodeling of κ as a function of p_T^{miss} , we assign an uncertainty based on the comparison between simulation and data at intermediate- and high- p_T^{miss} values for low M_J (high M_J) as 15 (19)% and 21 (30)%, respectively. These uncertainties contribute to the total uncertainty for each signal region, as summarized in Section 7.4.

7.3 Single-lepton, 5–6 jet control sample results

The single-lepton, 5–6 jet control sample (referred to simply as the 5–6 jet control sample) is constructed in a manner identical to the signal regions, except for the N_{jets} requirement. The κ values are studied in the low- and intermediate- p_T^{miss} bins, while the high- p_T^{miss} bin is not

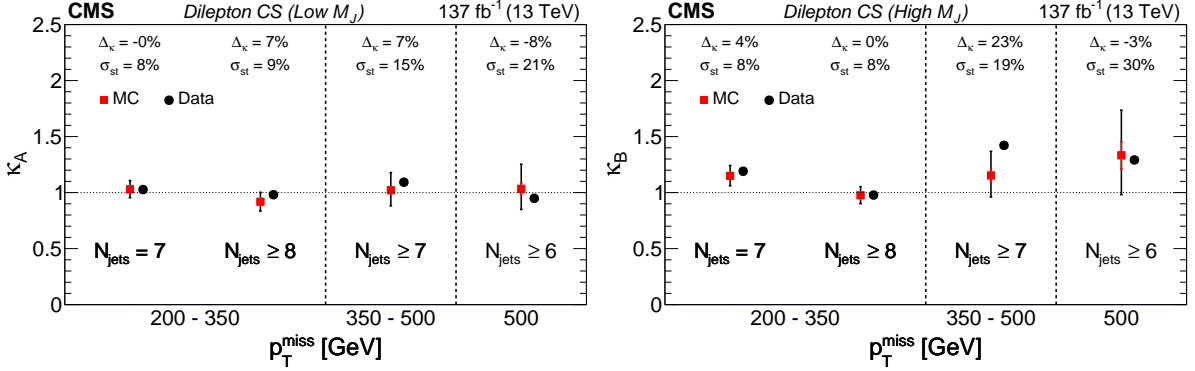


Figure 5: Dilepton control sample (CS): validation of the κ factor values found in simulation vs. data for low M_J (left) and high M_J (right). The data and simulation are shown as black and red points, respectively. No statistical uncertainties are plotted for the data points, but instead, the expected statistical uncertainty for the data points, summed in quadrature with the statistical uncertainty of the simulated samples, is given by the error bar on the red points and is quoted as σ_{st} . The red portion of the error bar on the red points indicates the contribution from the simulated samples. The quoted values of Δ_κ are defined as the relative difference between the κ values found in simulation and in data.

considered because of potential signal contamination (6-jet events are in fact part of the signal regions at high p_T^{miss}).

The κ measurement is performed in the three N_b bins at low p_T^{miss} and is also performed in the intermediate p_T^{miss} bin, integrating over N_b . Figure 6 compares the κ values obtained from simulation with those measured in the data. We find consistency between the simulation and the data except for a 3σ deviation in the 2 b-jet bin. Closer examination of distributions contributing to this κ value shows a higher yield in the region equivalent to R4A in the 5–6 jet control sample. Additional checks at $100 < p_T^{\text{miss}} \leq 200$ GeV for both 5–6 jet events and 7-jet events yield consistent κ values between the simulation and the data. These results, as well as studies of the shape of the N_b distribution, suggest that this discrepancy observed in the 2 b jet bin at low M_J is the result of a fluctuation. Nevertheless, we assign systematic uncertainties to cover potential mismodeling of κ as a function of N_b , taking 10, 20, and 25% as the uncertainties for events with $N_b = 1$, $N_b = 2$, and $N_b \geq 3$, respectively.

7.4 Summary of systematic uncertainties in the background estimate

Table 1 shows the total symmetrized systematic uncertainties in the κ values used to compute the background yields for each signal bin, based on the uncertainties derived in the control samples. These uncertainties are obtained by combining the uncertainties under the assumption of no correlation between any N_{jets} , N_b , and p_T^{miss} dependence as follows,

$$\begin{aligned}
 \sigma_{\text{low } p_T^{\text{miss}}, j, b}^{\text{SR}} &= \sigma_{\text{low } p_T^{\text{miss}}, b}^{5-6j} \oplus \sigma_{\text{low } p_T^{\text{miss}}, j}^{2\ell} \\
 \sigma_{\text{mid } p_T^{\text{miss}}, j, b}^{\text{SR}} &= \sigma_{\text{low } p_T^{\text{miss}}, b}^{5-6j} \oplus \sigma_{\text{low } p_T^{\text{miss}}, j}^{2\ell} \oplus \sigma_{\text{mid } p_T^{\text{miss}}, j}^{2\ell} \\
 \sigma_{\text{high } p_T^{\text{miss}}, j, b}^{\text{SR}} &= \sigma_{\text{low } p_T^{\text{miss}}, b}^{5-6j} \oplus \sigma_{\text{low } p_T^{\text{miss}}, j}^{2\ell} \oplus \sigma_{\text{high } p_T^{\text{miss}}, j}^{2\ell}
 \end{aligned} \tag{9}$$

where j and b are indices of the jet and b jet multiplicities, respectively. Here, $\sigma_{\text{low } p_T^{\text{miss}}, b}^{5-6j}$ refers to the uncertainty as a function of N_b derived in the low- p_T^{miss} bin of the single-lepton, 5–6 jet control sample; $\sigma_{\text{low } p_T^{\text{miss}}, j}^{2\ell}$ refers to the uncertainty as a function of N_{jets} derived in the low- p_T^{miss}

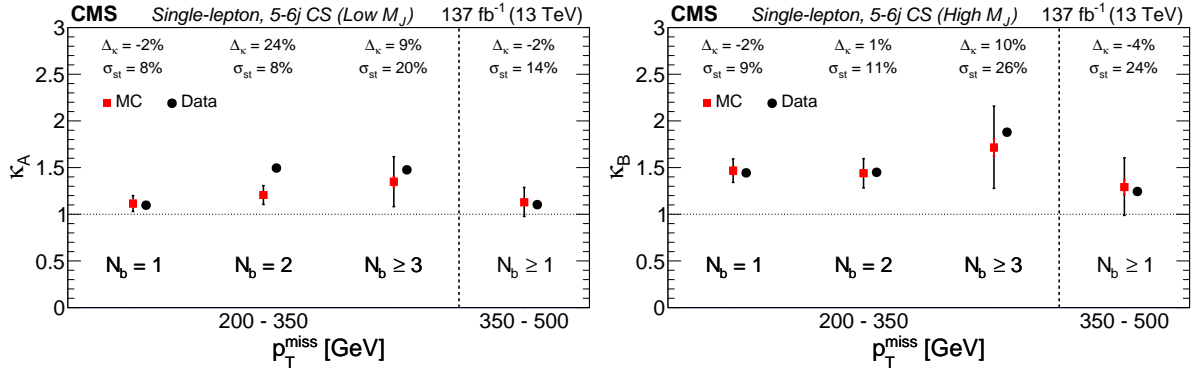


Figure 6: Single-lepton 5–6 jet CS: validation of the κ factor values found in simulation vs. data for low M_J (left) and high M_J (right). The data and simulation are shown as black and red points, respectively. The expected uncertainty in the data, summed in quadrature with the statistical uncertainty of the simulated samples, is given by the error bar on the red points (σ_{st}). The red portion of the error bar indicates the contribution from the simulated samples. The values of Δ_κ are the relative difference between the κ values found in simulation and in data.

Table 1: Systematic uncertainties in the background correction factors κ associated with each signal bin based on the control sample studies described in Sections 7.2 and 7.3 and combined according to Eq.(9).

	$200 < p_T^{\text{miss}} \leq 350 \text{ GeV}$			$350 < p_T^{\text{miss}} \leq 500 \text{ GeV}$			$p_T^{\text{miss}} > 500 \text{ GeV}$		
	$N_b = 1$	$N_b = 2$	$N_b \geq 3$	$N_b = 1$	$N_b = 2$	$N_b \geq 3$	$N_b = 1$	$N_b = 2$	$N_b \geq 3$
Low M_J	13%	22%	27%	20%	27%	31%	25%	30%	34%
High M_J	13%	22%	27%	22%	28%	32%	32%	36%	39%

bin of the dilepton control sample; and finally, $\sigma_{\text{mid } p_T^{\text{miss}}}^{2\ell}$ and $\sigma_{\text{high } p_T^{\text{miss}}}^{2\ell}$ refer to the uncertainty as a function of p_T^{miss} , integrated in N_{jets} and N_b , derived in the dilepton control sample. Since the uncertainty as a function of N_{jets} is derived in the low- p_T^{miss} bin of the dilepton sample, it already accounts for any mismodeling of the p_T^{miss} distribution at low p_T^{miss} , and thus no additional term is needed to account for such mismodeling in the first equation. Similarly, any mismodeling of the contribution of single-lepton mismeasured events at high m_T is already folded into the $\sigma_{\text{low } p_T^{\text{miss}, b}}^{5-6j}$ term, and thus no additional uncertainty is needed to account for this.

In practice, the three sources of uncertainty listed above are implemented in the likelihood as six log-normal constraints. A separate low- M_J and high- M_J nuisance parameter is assigned for each of the quantities $\sigma_{\text{low } p_T^{\text{miss}, j, b}}^{\text{SR}}$, $\sigma_{\text{mid } p_T^{\text{miss}, j, b}}^{\text{SR}}$ and $\sigma_{\text{high } p_T^{\text{miss}, j, b}}^{\text{SR}}$. The low- M_J and high- M_J nuisance parameters are decoupled, based on the observation that the background contributions for which $\kappa > 1$ have a p_T^{miss} dependence that is different at low M_J and high M_J . The total uncertainties with the full Run 2 data set are in the range 13 to 39%, increasing with p_T^{miss} .

8 Results and interpretation

Figure 7 shows two-dimensional distributions of the data in the M_J - m_T plane after applying the baseline selection described in Section 5, with separate plots for the intermediate- and high- p_T^{miss} bins. Both plots in the figure are integrated over N_{jets} and $N_b \geq 2$ and hence do not represent the full sensitivity of the analysis. Each event in data is represented by a single filled circle. For comparison, the plots also show the expected total SM background based

on simulation, as well as an illustrative sample of the simulated signal distribution for the T1tttt model with $m(\tilde{g}) = 2100$ GeV and $m(\tilde{\chi}_1^0) = 100$ GeV, plotted with one square per event, normalized to the same integrated luminosity as the data. This model has a large mass splitting between the gluino and the neutralino, and signal events typically have large values of p_T^{miss} . Qualitatively, the two-dimensional distribution of the data corresponds well to the expected distribution for the SM background events. The highest M_J , highest p_T^{miss} region shows several simulated signal events for the T1tttt(2100, 100) model. However, only two observed events populate this region in the data.

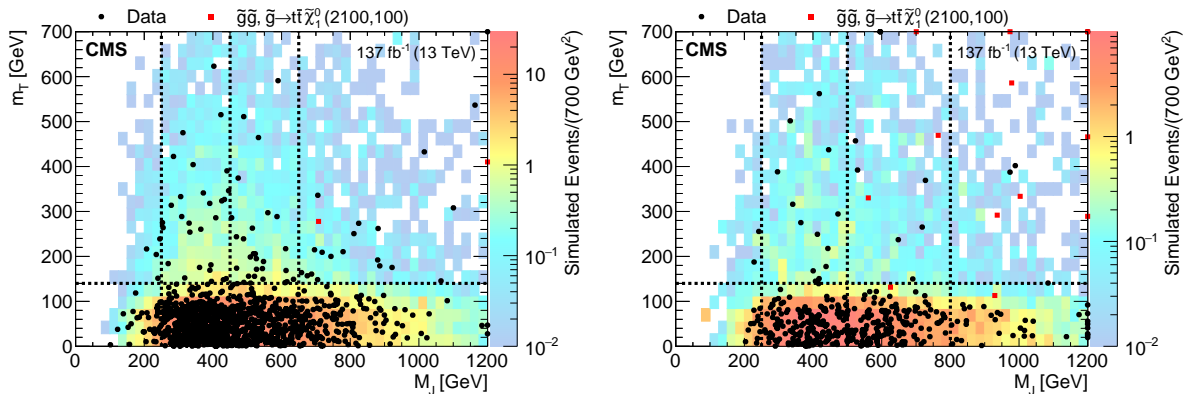


Figure 7: Two-dimensional distributions in M_J and m_T for both data and simulated event samples, integrated over the N_{jets} and $N_b \geq 2$ and shown separately for the $350 < p_T^{\text{miss}} \leq 500$ GeV bin (left) and the $p_T^{\text{miss}} > 500$ GeV bin (right). The black dots represent events in data, the colored histogram shows the total expected background yield per bin from simulation (not the actual predicted background), and the red squares correspond to a representative random sample of signal events drawn from the simulated distribution for the T1tttt model with $m(\tilde{g}) = 2100$ GeV and $m(\tilde{\chi}_1^0) = 100$ GeV for 137 fb^{-1} . Overflow events are shown on the edges of the plot.

The basic principle of the analysis is illustrated in Fig. 8, which compares, in three separate p_T^{miss} regions, the M_J distributions for low- m_T and high- m_T data. The low- m_T data correspond to regions R1, R2A, and R2B. Here, each event in R2A or R2B is weighted with the relevant κ factor, and then the total low- m_T yield is normalized to the total high- m_T yield in data. In the absence of signal, the shapes of these distributions should be approximately consistent, as observed. The low- and intermediate- p_T^{miss} regions (upper plots) show the background behavior with better statistical precision, while the high- p_T^{miss} region (bottom) has a higher sensitivity to the signal. For all three plots, integrals are performed over N_{jets} and N_b , as indicated in the legends.

Figure 9 shows the observed event yields in all of the signal regions and bins of the analysis, the predicted backgrounds with their uncertainties obtained from the R1–R3 and R1–R4 fits, and the pulls associated with the fits. Both the R1–R3 and the R1–R4 fits are based on the null hypothesis, i.e., no signal contribution. We observe a broad pattern of consistency between the observed data and predicted backgrounds in the search regions and bins. Most of the pulls are less than one standard deviation (s.d.). The largest pull is -2.0 s.d. and occurs in the bin with $M_J > 650$ GeV, $350 < p_T^{\text{miss}} \leq 500$ GeV, $N_{\text{jets}} = 7$, and $N_b = 1$.

Tables 2 (low M_J) and 3 (high M_J) present the same information as in Fig. 9, but in detailed numerical form, including the observed and fitted yields in regions R1–R3, as well as the expected signal yields for the two T1tttt benchmark model points. Again, the observed event yields in data are consistent with the background predictions.

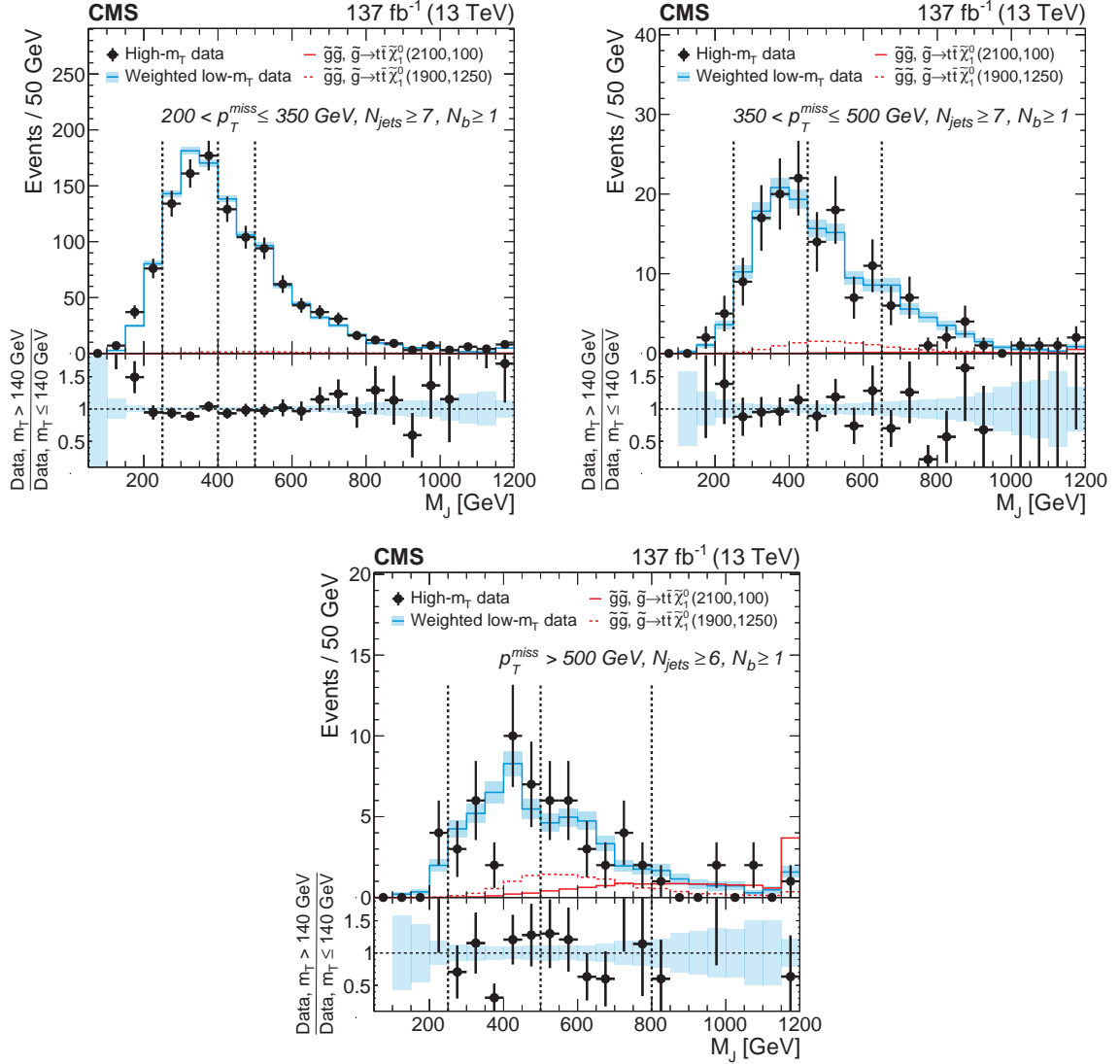


Figure 8: Distributions of M_J observed in data for $200 < p_T^{\text{miss}} \leq 350 \text{ GeV}$ (upper left), $350 < p_T^{\text{miss}} \leq 500 \text{ GeV}$ (upper right), and $p_T^{\text{miss}} > 500 \text{ GeV}$ (lower) in the 1ℓ data for low- and high- m_T regions. In each plot, events in the R2A and R2B regions at low m_T have been weighted by the relevant κ factor, and the total low- m_T yield is normalized to the high- m_T yield to facilitate comparison of the shapes of the distributions. The vertical dashed line at $M_J = 250 \text{ GeV}$ shows the lower boundary of regions R1 and R3, while the vertical lines at higher M_J values denote the lower M_J boundaries of the signal regions R4A and R4B. The data are integrated over the N_b and N_{jets} signal bins. Two SUSY benchmark models are shown in the solid and dashed red histograms.

Table 2: Observed and predicted event yields for the signal regions (R4A) and background regions (R1–R3) in the low- M_J ABCD planes. For the R1–R3 fit, the values given for R1, R2A and R3 correspond to the observed yields in those regions. Expected yields for the two SUSY benchmark scenarios, T1tttt(2100, 100) and T1tttt(1900, 1250), are also given. The uncertainties in the prediction account for the amount of data in the control samples, the precision of κ from MC, and the systematic uncertainties in κ assessed from control samples in data.

$\mathcal{L} = 137 \text{ fb}^{-1}$	T1tttt(2100,100)	T1tttt(1900,1250)	R1–R3 fit	R1–R4 fit	Observed
$200 < p_T^{\text{miss}} \leq 350 \text{ GeV}$					
R1	0.0	1.1	7706	7705 ± 87	7706
R2A: $N_b = 1, N_{\text{jets}} = 7$	0.0	0.1	1088	1088 ± 32	1088
R2A: $N_b = 1, N_{\text{jets}} \geq 8$	0.0	0.1	732	736 ± 26	732
R2A: $N_b = 2, N_{\text{jets}} = 7$	0.0	0.1	879	882 ± 30	879
R2A: $N_b = 2, N_{\text{jets}} \geq 8$	0.0	0.3	644	642 ± 25	644
R2A: $N_b \geq 3, N_{\text{jets}} = 7$	0.0	0.2	237	235 ± 15	237
R2A: $N_b \geq 3, N_{\text{jets}} \geq 8$	0.0	0.5	202	200 ± 14	202
R3	0.0	2.2	472	473 ± 20	472
R4A: $N_b = 1, N_{\text{jets}} = 7$	0.0	0.2	70 ± 10	70.2 ± 4.6	70
R4A: $N_b = 1, N_{\text{jets}} \geq 8$	0.0	0.3	37.7 ± 5.6	38.3 ± 2.8	42
R4A: $N_b = 2, N_{\text{jets}} = 7$	0.0	0.4	56 ± 12	55.7 ± 4.5	59
R4A: $N_b = 2, N_{\text{jets}} \geq 8$	0.0	0.6	37.9 ± 8.1	37.4 ± 3.1	35
R4A: $N_b \geq 3, N_{\text{jets}} = 7$	0.0	0.4	19.2 ± 4.9	18.7 ± 2.1	17
R4A: $N_b \geq 3, N_{\text{jets}} \geq 8$	0.0	0.9	12.9 ± 3.3	12.4 ± 1.5	10
$350 < p_T^{\text{miss}} \leq 500 \text{ GeV}$					
R1	0.0	0.9	967	968 ± 31	967
R2A: $N_b = 1, N_{\text{jets}} = 7$	0.0	0.1	208	207 ± 14	208
R2A: $N_b = 1, N_{\text{jets}} \geq 8$	0.0	0.2	150	148 ± 12	150
R2A: $N_b = 2, N_{\text{jets}} = 7$	0.0	0.1	139	142 ± 12	139
R2A: $N_b = 2, N_{\text{jets}} \geq 8$	0.0	0.3	111	112 ± 11	111
R2A: $N_b \geq 3, N_{\text{jets}} = 7$	0.0	0.2	30	30.1 ± 5.3	30
R2A: $N_b \geq 3, N_{\text{jets}} \geq 8$	0.0	0.6	38	37.7 ± 6.0	38
R3	0.1	2.9	68	67.0 ± 6.5	68
R4A: $N_b = 1, N_{\text{jets}} = 7$	0.1	0.3	15.2 ± 3.7	15.3 ± 2.1	14
R4A: $N_b = 1, N_{\text{jets}} \geq 8$	0.0	0.4	9.9 ± 2.7	9.7 ± 1.6	8
R4A: $N_b = 2, N_{\text{jets}} = 7$	0.1	0.5	10.8 ± 3.1	11.3 ± 1.7	14
R4A: $N_b = 2, N_{\text{jets}} \geq 8$	0.1	1.3	6.6 ± 1.9	6.8 ± 1.1	8
R4A: $N_b \geq 3, N_{\text{jets}} = 7$	0.1	0.7	2.8 ± 1.1	2.9 ± 0.7	3
R4A: $N_b \geq 3, N_{\text{jets}} \geq 8$	0.1	2.1	3.3 ± 1.2	3.3 ± 0.7	3
$p_T^{\text{miss}} > 500 \text{ GeV}$					
R1	0.1	0.6	434	434 ± 21	434
R2A: $N_b = 1, 6 \leq N_{\text{jets}} \leq 7$	0.1	0.1	158	160 ± 13	158
R2A: $N_b = 1, N_{\text{jets}} \geq 8$	0.0	0.2	41	41.7 ± 6.4	41
R2A: $N_b = 2, 6 \leq N_{\text{jets}} \leq 7$	0.1	0.2	80	80.5 ± 8.8	80
R2A: $N_b = 2, N_{\text{jets}} \geq 8$	0.1	0.3	34	32.0 ± 5.5	34
R2A: $N_b \geq 3, 6 \leq N_{\text{jets}} \leq 7$	0.1	0.2	20	19.8 ± 4.5	20
R2A: $N_b \geq 3, N_{\text{jets}} \geq 8$	0.1	0.5	10	10.1 ± 3.1	10
R3	0.6	3.2	28	27.9 ± 4.2	28
R4A: $N_b = 1, 6 \leq N_{\text{jets}} \leq 7$	0.6	0.5	9.4 ± 3.1	10.2 ± 1.9	12
R4A: $N_b = 1, N_{\text{jets}} \geq 8$	0.3	0.5	2.1 ± 0.8	2.3 ± 0.6	3
R4A: $N_b = 2, 6 \leq N_{\text{jets}} \leq 7$	0.9	1.0	5.3 ± 2.0	5.5 ± 1.1	6
R4A: $N_b = 2, N_{\text{jets}} \geq 8$	0.6	1.3	2.1 ± 0.9	2.0 ± 0.5	0
R4A: $N_b \geq 3, 6 \leq N_{\text{jets}} \leq 7$	0.8	0.9	1.2 ± 0.6	1.2 ± 0.4	1
R4A: $N_b \geq 3, N_{\text{jets}} \geq 8$	0.8	2.3	0.8 ± 0.4	0.9 ± 0.3	1

Table 3: Observed and predicted event yields for the signal regions (R4B) and background regions (R1–R3) in the high- M_J ABCD planes. For the R1–R3 fit, the values given for R1, R2B and R3 correspond to the observed yields in those regions. Expected yields for the two SUSY benchmark scenarios, T1tttt(2100, 100) and T1tttt(1900, 1250), are also given. The uncertainties in the prediction account for the amount of data in the control samples, the precision of κ from MC, and the systematic uncertainties in κ assessed from control samples in data.

$\mathcal{L} = 137 \text{ fb}^{-1}$	T1tttt(2100,100)	T1tttt(1900,1250)	R1–R3 fit	R1–R4 fit	Observed
$200 < p_T^{\text{miss}} \leq 350 \text{ GeV}$					
R1	0.0	1.1	7706	7705 ± 87	7706
R2B: $N_b = 1, N_{\text{jets}} = 7$	0.0	0.1	935	937 ± 30	935
R2B: $N_b = 1, N_{\text{jets}} \geq 8$	0.1	0.3	961	959 ± 30	961
R2B: $N_b = 2, N_{\text{jets}} = 7$	0.0	0.2	600	606 ± 24	600
R2B: $N_b = 2, N_{\text{jets}} \geq 8$	0.1	0.6	832	821 ± 28	832
R2B: $N_b \geq 3, N_{\text{jets}} = 7$	0.0	0.2	168	171 ± 13	168
R2B: $N_b \geq 3, N_{\text{jets}} \geq 8$	0.1	1.1	306	308 ± 17	306
R3	0.0	2.2	472	473 ± 20	472
R4B: $N_b = 1, N_{\text{jets}} = 7$	0.1	0.2	76 ± 11	81.7 ± 5.6	84
R4B: $N_b = 1, N_{\text{jets}} \geq 8$	0.2	0.5	72 ± 10	76.3 ± 4.9	74
R4B: $N_b = 2, N_{\text{jets}} = 7$	0.2	0.4	49 ± 10	57.6 ± 4.3	64
R4B: $N_b = 2, N_{\text{jets}} \geq 8$	0.3	1.5	63 ± 13	70.0 ± 5.1	59
R4B: $N_b \geq 3, N_{\text{jets}} = 7$	0.1	0.6	15.2 ± 3.9	18.8 ± 2.1	22
R4B: $N_b \geq 3, N_{\text{jets}} \geq 8$	0.4	2.6	24.9 ± 6.1	30.1 ± 2.9	32
$350 < p_T^{\text{miss}} \leq 500 \text{ GeV}$					
R1	0.0	0.9	967	968 ± 31	967
R2B: $N_b = 1, N_{\text{jets}} = 7$	0.0	0.0	78	72.2 ± 8.2	78
R2B: $N_b = 1, N_{\text{jets}} \geq 8$	0.1	0.1	95	92.4 ± 9.5	95
R2B: $N_b = 2, N_{\text{jets}} = 7$	0.1	0.0	54	55.8 ± 7.3	54
R2B: $N_b = 2, N_{\text{jets}} \geq 8$	0.1	0.2	65	66.1 ± 8.1	65
R2B: $N_b \geq 3, N_{\text{jets}} = 7$	0.0	0.1	8	9.1 ± 2.9	8
R2B: $N_b \geq 3, N_{\text{jets}} \geq 8$	0.1	0.4	16	18.7 ± 4.2	16
R3	0.1	2.9	68	67.0 ± 6.5	68
R4B: $N_b = 1, N_{\text{jets}} = 7$	0.2	0.1	8.7 ± 2.6	6.8 ± 1.4	1
R4B: $N_b = 1, N_{\text{jets}} \geq 8$	0.2	0.3	8.4 ± 2.4	7.6 ± 1.4	5
R4B: $N_b = 2, N_{\text{jets}} = 7$	0.2	0.1	4.7 ± 1.6	5.2 ± 1.0	7
R4B: $N_b = 2, N_{\text{jets}} \geq 8$	0.4	0.7	4.6 ± 1.5	4.9 ± 0.9	6
R4B: $N_b \geq 3, N_{\text{jets}} = 7$	0.2	0.1	0.7 ± 0.4	0.9 ± 0.3	2
R4B: $N_b \geq 3, N_{\text{jets}} \geq 8$	0.5	1.3	1.8 ± 0.8	2.3 ± 0.7	5
$p_T^{\text{miss}} > 500 \text{ GeV}$					
R1	0.1	0.6	434	434 ± 21	434
R2B: $N_b = 1, 6 \leq N_{\text{jets}} \leq 7$	0.1	0.0	49	46.9 ± 7.0	49
R2B: $N_b = 1, N_{\text{jets}} \geq 8$	0.2	0.1	13	13.2 ± 3.7	13
R2B: $N_b = 2, 6 \leq N_{\text{jets}} \leq 7$	0.2	0.0	18	18.5 ± 4.3	18
R2B: $N_b = 2, N_{\text{jets}} \geq 8$	0.3	0.2	7	7.6 ± 2.8	7
R2B: $N_b \geq 3, 6 \leq N_{\text{jets}} \leq 7$	0.2	0.0	4	4.5 ± 2.1	4
R2B: $N_b \geq 3, N_{\text{jets}} \geq 8$	0.4	0.3	5	4.3 ± 2.0	5
R3	0.6	3.2	28	27.9 ± 4.2	28
R4B: $N_b = 1, 6 \leq N_{\text{jets}} \leq 7$	1.0	0.1	3.7 ± 1.5	3.1 ± 0.9	1
R4B: $N_b = 1, N_{\text{jets}} \geq 8$	1.1	0.3	0.8 ± 0.4	0.8 ± 0.3	1
R4B: $N_b = 2, 6 \leq N_{\text{jets}} \leq 7$	1.4	0.1	1.5 ± 0.7	1.5 ± 0.5	2
R4B: $N_b = 2, N_{\text{jets}} \geq 8$	2.0	0.6	0.3 ± 0.2	0.4 ± 0.2	1
R4B: $N_b \geq 3, 6 \leq N_{\text{jets}} \leq 7$	1.1	0.1	0.4 ± 0.3	0.5 ± 0.3	1
R4B: $N_b \geq 3, N_{\text{jets}} \geq 8$	2.4	1.0	0.9 ± 0.6	0.7 ± 0.4	0

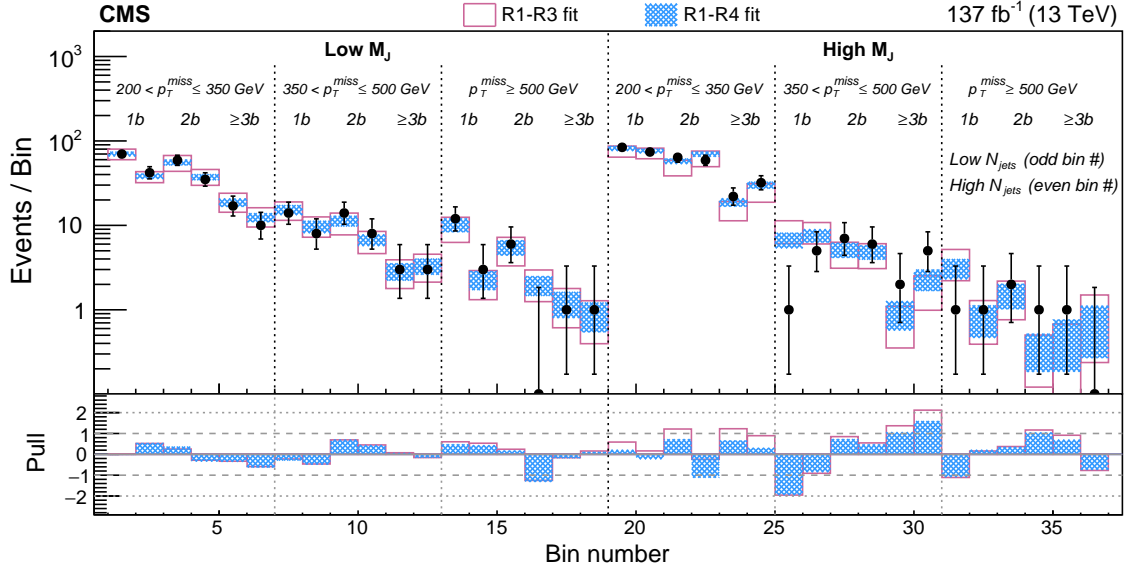


Figure 9: Observed and predicted event yields in each signal region. The open rectangles represent the prediction and uncertainty obtained using event yields from regions R1, R2, and R3 only (R1–R3 fit), while the hashed rectangles represent the prediction obtained when all regions are included in the fit (R1–R4 fit). The labels 1b, 2b, and $\geq 3b$ refer to $N_b = 1$, $N_b = 2$, and $N_b \geq 3$ bins, respectively. In both cases, all statistical and systematic uncertainties are included. The bottom panel shows the pulls for both fits, defined as $(N_{\text{obs}} - N_{\text{pred}}) / \sqrt{N_{\text{pred}} + (\sigma_{\text{pred}}^{\text{sys}})^2}$.

The results are first interpreted in terms of the simplified model T1tttt of SUSY particle production. This model is characterized by just two mass parameters, $m(\tilde{g})$ and $m(\tilde{\chi}_1^0)$. To determine which sets of masses, or mass points, are excluded by the data, we generate a set of simulated signal samples in which the mass parameters are varied across the range to which the analysis is potentially sensitive. These samples are used to determine the number of events that would be expected at each mass point, given the theoretical production cross section for this point. To assess which model points can be excluded by the data, it is necessary to evaluate the systematic uncertainties associated with the expected number of observed signal events.

Systematic uncertainties in the expected signal yields account for uncertainties in the trigger, lepton identification, jet identification, and b tagging efficiencies in simulated events; uncertainties in the distributions of p_T^{miss} , number of pileup vertices, and ISR jet multiplicity; and uncertainties in the jet energy corrections, renormalization and factorization scales, and integrated luminosity [88–90]. Each systematic uncertainty is evaluated in each of the analysis bins separately, and the uncertainties are treated as symmetric log-normal distributions. In the case that the sizes of up and down variations are not the same, the variation having larger absolute value is taken. If the sign of variations changes bin-by-bin, the correlation between bins is preserved, while the value that has the larger absolute variation is taken. A summary of the magnitude of the uncertainty due to each systematic source across sensitive signal bins for each of the two signal benchmark points is shown in Table 4.

An upper limit on the production cross section at 95% confidence level (CL) is estimated using the modified frequentist CL_s method [91–93], with a one-sided profile likelihood ratio test statistic, using an asymptotic approximation [94]. The statistical uncertainties from data counts in the control regions are modeled by Poisson terms. All systematic uncertainties are multiplicative and are treated as log-normal distributions. Exclusion limits are also estimated for ± 1 s.d. variations on the production cross section based on the approximate NNLO+NNLL

Table 4: Range of values for the systematic uncertainties in the signal efficiency and acceptance across sensitive bins, specifically across high p_T^{miss} signal bins for T1tttt(2100,100) and high N_{jets} signal bins for T1tttt(1900,1250). Uncertainties due to a particular source are treated as fully correlated among bins, while uncertainties due to different sources are treated as uncorrelated.

Source	Relative uncertainty [%]	
	T1tttt(2100,100)	T1tttt(1900,1250)
MC sample size	3–8	7–15
Renormalization and factorization scales	1–2	2–4
Fast MC p_T^{miss} resolution	1–2	1–5
Lepton efficiency	7–9	4–5
Trigger efficiency	1	1
b tagging efficiency	2–8	2–8
Mistag efficiency	1	1–3
Jet energy corrections	1–5	2–11
Initial-state radiation	1–7	1–10
Jet identification	1	1
Pileup	1–2	1–4
Integrated luminosity	2.3–2.5	2.3–2.5

calculation.

Figures 10 and 11 show the corresponding excluded cross section regions at 95% CL for the T1tttt and T5tttt models, respectively, in the $m(\tilde{g})$ - $m(\tilde{\chi}_1^0)$ plane. These regions correspond to excluded cross sections under the assumption that the branching fraction for the given process is 100%. For T1tttt, gluinos with masses of up to approximately 2150 GeV are excluded for $\tilde{\chi}_1^0$ masses up to about 700 GeV. The highest limit on the $\tilde{\chi}_1^0$ mass is approximately 1250 GeV, attained for $m(\tilde{g})$ of about 1700–1900 GeV. The observed limits for T1tttt are within the 1σ uncertainty of the expected limits across the full scan range.

The T5tttt model allows us to extend the interpretation of the results to scenarios in which the top squark is lighter than the gluino. Rather than considering a large set of models with independently varying top squark masses, we consider the extreme case in which the top squark has approximately the smallest mass consistent with two-body decay, $m(\tilde{t}) \approx m(t) + m(\tilde{\chi}_1^0)$, for a range of gluino and neutralino masses. The decay kinematics for such extreme, compressed mass spectrum models correspond to the lowest signal efficiency for given values of $m(\tilde{g})$ and $m(\tilde{\chi}_1^0)$, because the top quark and the $\tilde{\chi}_1^0$ are produced at rest in the top squark frame. As a consequence, the excluded signal cross section for fixed values of $m(\tilde{g})$ and $m(\tilde{\chi}_1^0)$ and with $m(\tilde{g}) > m(\tilde{t}_1) \geq m(t) + m(\tilde{\chi}_1^0)$ is minimized for this extreme model point. In particular, at low $m(\tilde{\chi}_1^0)$ the neutralino carries very little momentum, thus reducing the value of m_T , and resulting in significantly lower sensitivity for T5tttt than T1tttt. In this kinematic region, the sensitivity to the signal is in fact dominated by the events that have at least two leptonic W boson decays, which produce additional p_T^{miss} , as well as a tail in the m_T distribution. Although such dilepton events are nominally excluded in the analysis, a significant number of these signal events escape the dilepton veto.

For physical consistency, the signal model used in the T5tttt study should include not only gluino pair production, but also direct top squark pair production, $\tilde{t}\tilde{t}$, referred to as T2tt. For $m(\tilde{\chi}_1^0) < 33$ GeV and $100 < m(\tilde{\chi}_1^0) < 550$ GeV, with $m(\tilde{t}) - m(\tilde{\chi}_1^0) = 175$ GeV, the T2tt model

is excluded in direct searches for $\tilde{t}\tilde{t}$ production [72, 95]. For $33 < m(\tilde{\chi}_1^0) < 100$ GeV, the T2tt model is not excluded due to the difficulty in assessing the rapidly changing acceptance with the finite event count available in simulation. We have verified that for $m(\tilde{\chi}_1^0) > 550$ GeV, where the T2tt model remains unexcluded, adding the contribution from the T2tt process to our analysis regions does not have a significant effect on the sensitivity. For simplicity, in Fig. 11, we have based the exclusion curve on T5ttt only, without including the additional T2tt process.

As with all SUSY particle mass limits obtained in the context of simplified models, it is important to recognize that the results can be significantly weakened if the assumptions of the model fail to hold. In particular, the presence of alternative decay modes could reduce the number of expected events for the given selection. However, cross section limits remain valid if they are interpreted as limits on cross section multiplied by the branching fraction for the assumed decay mode.

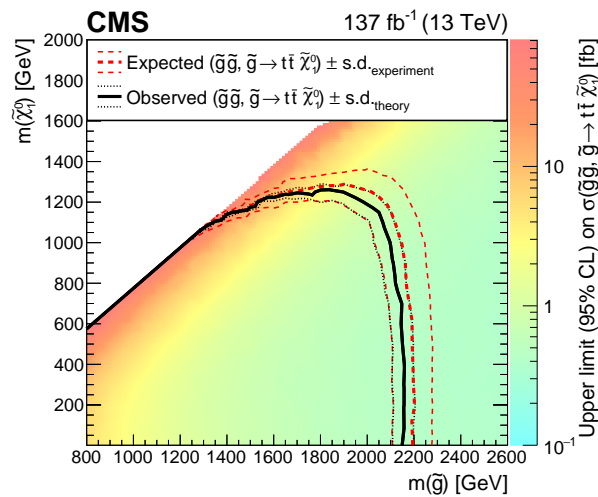


Figure 10: Interpretation of the results in the T1ttt model. The colored regions show the upper limits (95% CL) on the production cross section for $pp \rightarrow \tilde{g}\tilde{g}, \tilde{g} \rightarrow \tilde{t}\tilde{t}\tilde{\chi}_1^0$ in the $m(\tilde{g})$ - $m(\tilde{\chi}_1^0)$ plane. The curves show the expected and observed limits on the corresponding SUSY particle masses obtained by comparing the excluded cross section with theoretical cross sections.

9 Summary

A search is performed for an excess event yield above that expected for standard model processes using a data sample of proton-proton collision events with an integrated luminosity of 137 fb^{-1} at $\sqrt{s} = 13$ TeV. The experimental signature is characterized by a single isolated lepton, multiple jets, at least one b-tagged jet, and large missing transverse momentum. No significant excesses above the standard model backgrounds are observed. The results are interpreted in the framework of simplified models that describe natural supersymmetry scenarios. For gluino pair production followed by the three-body decay $\tilde{g} \rightarrow \tilde{t}\tilde{t}\tilde{\chi}_1^0$ (T1ttt model), gluinos with masses below about 2150 GeV are excluded at 95% confidence level for neutralino masses up to 700 GeV. The highest excluded neutralino mass is about 1250 GeV. For the two-body gluino decay $\tilde{g} \rightarrow \tilde{t}_1\tilde{t}$ with $\tilde{t}_1 \rightarrow \tilde{t}\tilde{\chi}_1^0$ (T5ttt model), the results are generally similar, except at low neutralino masses, where the excluded gluino mass is somewhat lower. These results extend previous gluino mass limits [19] from this search by about 250 GeV, due to both the data sample increase and the analysis reoptimization enabled by it. These mass limits are among the most stringent constraints on this supersymmetry model to date.

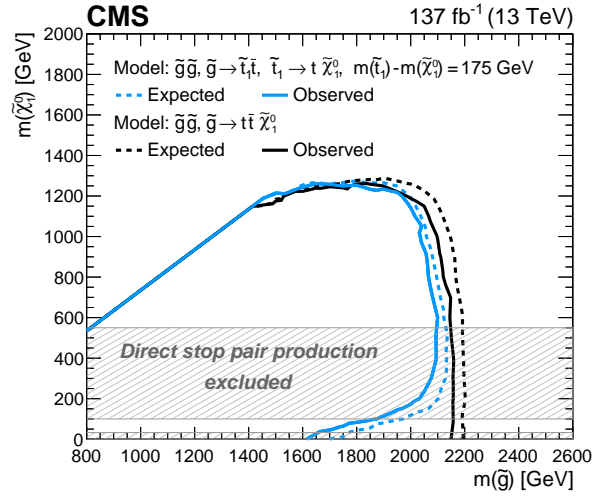


Figure 11: Interpretation of the results in the T5tttt model. The expected and observed upper limits do not take into account contributions from direct top squark pair production; however, its effect for $m(\tilde{\chi}_1^0) > 550$ GeV is small. The T1tttt interpretation results are also shown for comparison.

Acknowledgments

We congratulate our colleagues in the CERN accelerator departments for the excellent performance of the LHC and thank the technical and administrative staffs at CERN and at other CMS institutes for their contributions to the success of the CMS effort. In addition, we gratefully acknowledge the computing centres and personnel of the Worldwide LHC Computing Grid for delivering so effectively the computing infrastructure essential to our analyses. Finally, we acknowledge the enduring support for the construction and operation of the LHC and the CMS detector provided by the following funding agencies: BMBWF and FWF (Austria); FNRS and FWO (Belgium); CNPq, CAPES, FAPERJ, FAPERGS, and FAPESP (Brazil); MES (Bulgaria); CERN; CAS, MoST, and NSFC (China); COLCIENCIAS (Colombia); MSES and CSF (Croatia); RPF (Cyprus); SENESCYT (Ecuador); MoER, ERC IUT, PUT and ERDF (Estonia); Academy of Finland, MEC, and HIP (Finland); CEA and CNRS/IN2P3 (France); BMBF, DFG, and HGF (Germany); GSRT (Greece); NKFIA (Hungary); DAE and DST (India); IPM (Iran); SFI (Ireland); INFN (Italy); MSIP and NRF (Republic of Korea); MES (Latvia); LAS (Lithuania); MOE and UM (Malaysia); BUAP, CINVESTAV, CONACYT, LNS, SEP, and UASLP-FAI (Mexico); MOS (Montenegro); MBIE (New Zealand); PAEC (Pakistan); MSHE and NSC (Poland); FCT (Portugal); JINR (Dubna); MON, RosAtom, RAS, RFBR, and NRC KI (Russia); MESTD (Serbia); SEIDI, CPAN, PCTI, and FEDER (Spain); MOSTR (Sri Lanka); Swiss Funding Agencies (Switzerland); MST (Taipei); ThEPCenter, IPST, STAR, and NSTDA (Thailand); TUBITAK and TAEK (Turkey); NASU (Ukraine); STFC (United Kingdom); DOE and NSF (USA).

Individuals have received support from the Marie-Curie programme and the European Research Council and Horizon 2020 Grant, contract Nos. 675440, 752730, and 765710 (European Union); the Leventis Foundation; the A.P. Sloan Foundation; the Alexander von Humboldt Foundation; the Belgian Federal Science Policy Office; the Fonds pour la Formation à la Recherche dans l'Industrie et dans l'Agriculture (FRIA-Belgium); the Agentschap voor Innovatie door Wetenschap en Technologie (IWT-Belgium); the F.R.S.-FNRS and FWO (Belgium) under the "Excellence of Science – EOS" – be.h project n. 30820817; the Beijing Municipal Science & Technology Commission, No. Z181100004218003; the Ministry of Education, Youth and Sports (MEYS) of the Czech Republic; the Deutsche Forschungsgemeinschaft (DFG) under Ger-

manys Excellence Strategy EXC 2121 “Quantum Universe” – 390833306; the Lendület (“Momentum”) Programme and the János Bolyai Research Scholarship of the Hungarian Academy of Sciences, the New National Excellence Program ÚNKP, the NKfIA research grants 123842, 123959, 124845, 124850, 125105, 128713, 128786, and 129058 (Hungary); the Council of Science and Industrial Research, India; the HOMING PLUS programme of the Foundation for Polish Science, cofinanced from European Union, Regional Development Fund, the Mobility Plus programme of the Ministry of Science and Higher Education, the National Science Center (Poland), contracts Harmonia 2014/14/M/ST2/00428, Opus 2014/13/B/ST2/02543, 2014/15/B/ST2/03998, and 2015/19/B/ST2/02861, Sonata-bis 2012/07/E/ST2/01406; the National Priorities Research Program by Qatar National Research Fund; the Ministry of Science and Education, grant no. 3.2989.2017 (Russia); the Programa Estatal de Fomento de la Investigación Científica y Técnica de Excelencia María de Maeztu, grant MDM-2015-0509 and the Programa Severo Ochoa del Principado de Asturias; the Thalís and Aristeia programmes cofinanced by EU-ESF and the Greek NSRF; the Rachadapisek Sompot Fund for Postdoctoral Fellowship, Chulalongkorn University and the Chulalongkorn Academic into Its 2nd Century Project Advancement Project (Thailand); the Nvidia Corporation; the Welch Foundation, contract C-1845; and the Weston Havens Foundation (USA).

References

- [1] L. Evans and P. Bryant, “LHC machine”, *JINST* **3** S08001, doi:10.1088/1748-0221/3/08/S08001.
- [2] P. Ramond, “Dual theory for free fermions”, *Phys. Rev. D* **3** (1971) 2415, doi:10.1103/PhysRevD.3.2415.
- [3] Y. A. Gol’fand and E. P. Likhtman, “Extension of the algebra of Poincaré group generators and violation of P invariance”, *JETP Lett.* **13** (1971) 323.
- [4] A. Neveu and J. H. Schwarz, “Factorizable dual model of pions”, *Nucl. Phys. B* **31** (1971) 86, doi:10.1016/0550-3213(71)90448-2.
- [5] D. V. Volkov and V. P. Akulov, “Possible universal neutrino interaction”, *JETP Lett.* **16** (1972) 438.
- [6] J. Wess and B. Zumino, “A lagrangian model invariant under supergauge transformations”, *Phys. Lett. B* **49** (1974) 52, doi:10.1016/0370-2693(74)90578-4.
- [7] J. Wess and B. Zumino, “Supergauge transformations in four dimensions”, *Nucl. Phys. B* **70** (1974) 39, doi:10.1016/0550-3213(74)90355-1.
- [8] P. Fayet, “Supergauge invariant extension of the Higgs mechanism and a model for the electron and its neutrino”, *Nucl. Phys. B* **90** (1975) 104, doi:10.1016/0550-3213(75)90636-7.
- [9] H. P. Nilles, “Supersymmetry, supergravity and particle physics”, *Phys. Rep.* **110** (1984) 1, doi:10.1016/0370-1573(84)90008-5.
- [10] ATLAS Collaboration, “Search for supersymmetry in final states with jets, missing transverse momentum and one isolated lepton in $\sqrt{s} = 7$ TeV pp collisions using 1 fb⁻¹ of ATLAS data”, *Phys. Rev. D* **85** (2012) 012006, doi:10.1103/PhysRevD.85.012006, arXiv:1109.6606. [Erratum: doi:10.1103/PhysRevD.87.099903].

-
- [11] ATLAS Collaboration, “Search for squarks and gluinos in events with isolated leptons, jets and missing transverse momentum at $\sqrt{s} = 8$ TeV with the ATLAS detector”, *JHEP* **04** (2015) 116, doi:10.1007/JHEP04(2015)116, arXiv:1501.03555.
- [12] CMS Collaboration, “Search for supersymmetry in pp collisions at $\sqrt{s} = 7$ TeV in events with a single lepton, jets, and missing transverse momentum”, *JHEP* **08** (2011) 156, doi:10.1007/JHEP08(2011)156, arXiv:1107.1870.
- [13] CMS Collaboration, “Search for supersymmetry in pp collisions at $\sqrt{s} = 8$ TeV in events with a single lepton, large jet multiplicity, and multiple b jets”, *Phys. Lett. B* **733** (2014) 328, doi:10.1016/j.physletb.2014.04.023, arXiv:1311.4937.
- [14] ATLAS Collaboration, “Search for pair production of gluinos decaying via stop and sbottom in events with b-jets and large missing transverse momentum in pp collisions at $\sqrt{s} = 13$ TeV with the ATLAS detector”, *Phys. Rev. D* **94** (2016) 032003, doi:10.1103/PhysRevD.94.032003, arXiv:1605.09318.
- [15] ATLAS Collaboration, “Search for gluinos in events with an isolated lepton, jets and missing transverse momentum at $\sqrt{s} = 13$ TeV with the ATLAS detector”, *Eur. Phys. J. C* **76** (2016) 565, doi:10.1140/epjc/s10052-016-4397-x, arXiv:1605.04285.
- [16] ATLAS Collaboration, “Search for supersymmetry in final states with missing transverse momentum and multiple b-jets in proton-proton collisions at $\sqrt{s} = 13$ TeV with the ATLAS detector”, *JHEP* **06** (2018) 107, doi:10.1007/JHEP06(2018)107, arXiv:1711.01901.
- [17] CMS Collaboration, “Search for supersymmetry in pp collisions at $\sqrt{s} = 13$ TeV in the single-lepton final state using the sum of masses of large-radius jets”, *JHEP* **08** (2016) 122, doi:10.1007/JHEP08(2016)122, arXiv:1605.04608.
- [18] CMS Collaboration, “Search for supersymmetry in events with one lepton and multiple jets in proton-proton collisions at $\sqrt{s} = 13$ TeV”, *Phys. Rev. D* **95** (2017) 012011, doi:10.1103/PhysRevD.95.012011, arXiv:1609.09386.
- [19] CMS Collaboration, “Search for supersymmetry in pp collisions at $\sqrt{s} = 13$ TeV in the single-lepton final state using the sum of masses of large-radius jets”, *Phys. Rev. Lett.* **119** (2017) 151802, doi:10.1103/PhysRevLett.119.151802, arXiv:1705.04673.
- [20] ATLAS Collaboration, “Observation of a new particle in the search for the standard model Higgs boson with the ATLAS detector at the LHC”, *Phys. Lett. B* **716** (2012) 1, doi:10.1016/j.physletb.2012.08.020, arXiv:1207.7214.
- [21] CMS Collaboration, “Observation of a new boson at a mass of 125 GeV with the CMS experiment at the LHC”, *Phys. Lett. B* **716** (2012) 30, doi:10.1016/j.physletb.2012.08.021, arXiv:1207.7235.
- [22] CMS Collaboration, “Observation of a new boson with mass near 125 GeV in pp collisions at $\sqrt{s} = 7$ and 8 TeV”, *JHEP* **06** (2013) 081, doi:10.1007/JHEP06(2013)081, arXiv:1303.4571.
- [23] CMS Collaboration, “Precise determination of the mass of the Higgs boson and tests of compatibility of its couplings with the standard model predictions using proton collisions at 7 and 8 TeV”, *Eur. Phys. J. C* **75** (2015) 212, doi:10.1140/epjc/s10052-015-3351-7, arXiv:1412.8662.

- [24] ATLAS Collaboration, “Measurement of the Higgs boson mass from the $H \rightarrow \gamma\gamma$ and $H \rightarrow ZZ^* \rightarrow 4\ell$ channels with the ATLAS detector using 25 fb^{-1} of pp collision data”, *Phys. Rev. D* **90** (2014) 052004, doi:10.1103/PhysRevD.90.052004, arXiv:1406.3827.
- [25] ATLAS and CMS Collaborations, “Combined measurement of the Higgs boson mass in pp collisions at $\sqrt{s} = 7$ and 8 TeV with the ATLAS and CMS experiments”, *Phys. Rev. Lett.* **114** (2015) 191803, doi:10.1103/PhysRevLett.114.191803, arXiv:1503.07589.
- [26] G. 't Hooft, “Naturalness, chiral symmetry, and spontaneous chiral symmetry breaking”, *NATO Sci. Ser. B* **59** (1980) 135, doi:10.1007/978-1-4684-7571-5_9.
- [27] E. Witten, “Dynamical breaking of supersymmetry”, *Nucl. Phys. B* **188** (1981) 513, doi:10.1016/0550-3213(81)90006-7.
- [28] M. Dine, W. Fischler, and M. Srednicki, “Supersymmetric technicolor”, *Nucl. Phys. B* **189** (1981) 575, doi:10.1016/0550-3213(81)90582-4.
- [29] S. Dimopoulos and S. Raby, “Supercolor”, *Nucl. Phys. B* **192** (1981) 353, doi:10.1016/0550-3213(81)90430-2.
- [30] S. Dimopoulos and H. Georgi, “Softly broken supersymmetry and SU(5)”, *Nucl. Phys. B* **193** (1981) 150, doi:10.1016/0550-3213(81)90522-8.
- [31] R. K. Kaul and P. Majumdar, “Cancellation of quadratically divergent mass corrections in globally supersymmetric spontaneously broken gauge theories”, *Nucl. Phys. B* **199** (1982) 36, doi:10.1016/0550-3213(82)90565-X.
- [32] R. Barbieri and G. F. Giudice, “Upper bounds on supersymmetric particle masses”, *Nucl. Phys. B* **306** (1988) 63, doi:10.1016/0550-3213(88)90171-X.
- [33] S. Dimopoulos and G. F. Giudice, “Naturalness constraints in supersymmetric theories with nonuniversal soft terms”, *Phys. Lett. B* **357** (1995) 573, doi:10.1016/0370-2693(95)00961-J, arXiv:hep-ph/9507282.
- [34] R. Barbieri and D. Pappadopulo, “S-particles at their naturalness limits”, *JHEP* **10** (2009) 061, doi:10.1088/1126-6708/2009/10/061, arXiv:0906.4546.
- [35] M. Papucci, J. T. Ruderman, and A. Weiler, “Natural SUSY endures”, *JHEP* **09** (2012) 035, doi:10.1007/JHEP09(2012)035, arXiv:1110.6926.
- [36] J. L. Feng, “Naturalness and the status of supersymmetry”, *Ann. Rev. Nucl. Part. Sci.* **63** (2013) 351, doi:10.1146/annurev-nucl-102010-130447, arXiv:1302.6587.
- [37] G. R. Farrar and P. Fayet, “Phenomenology of the production, decay, and detection of new hadronic states associated with supersymmetry”, *Phys. Lett. B* **76** (1978) 575, doi:10.1016/0370-2693(78)90858-4.
- [38] S. P. Martin, “A supersymmetry primer”, *Adv. Ser. Direct. High Energy Phys.* **18** (1998) 1, doi:10.1142/9789812839657_0001, arXiv:hep-ph/9709356.
- [39] F. Zwicky, “Die rotverschiebung von extragalaktischen nebeln”, *Helv. Phys. Acta* **6** (1933) 110, doi:10.1007/s10714-008-0707-4.

-
- [40] V. C. Rubin and W. K. Ford Jr, "Rotation of the Andromeda nebula from a spectroscopic survey of emission regions", *Astrophys. J.* **159** (1970) 379, doi:10.1086/150317.
- [41] Particle Data Group, M. Tanabashi et al., "Review of particle physics", *Phys. Rev. D* **98** (2018) 030001, doi:10.1103/PhysRevD.98.030001.
- [42] CMS Collaboration, "Interpretation of searches for supersymmetry with simplified models", *Phys. Rev. D* **88** (2013) 052017, doi:10.1103/PhysRevD.88.052017, arXiv:1301.2175.
- [43] J. Alwall, P. C. Schuster, and N. Toro, "Simplified models for a first characterization of new physics at the LHC", *Phys. Rev. D* **79** (2009) 075020, doi:10.1103/PhysRevD.79.075020, arXiv:0810.3921.
- [44] J. Alwall, M.-P. Le, M. Lisanti, and J. G. Wacker, "Model-independent jets plus missing energy searches", *Phys. Rev. D* **79** (2009) 015005, doi:10.1103/PhysRevD.79.015005, arXiv:0809.3264.
- [45] D. Alves et al., "Simplified models for LHC new physics searches", *J. Phys. G* **39** (2012) 105005, doi:10.1088/0954-3899/39/10/105005, arXiv:1105.2838.
- [46] A. Hook, E. Izaguirre, M. Lisanti, and J. G. Wacker, "High multiplicity searches at the LHC using jet masses", *Phys. Rev. D* **85** (2012) 055029, doi:10.1103/PhysRevD.85.055029, arXiv:1202.0558.
- [47] T. Cohen, E. Izaguirre, M. Lisanti, and H. K. Lou, "Jet substructure by accident", *JHEP* **03** (2013) 161, doi:10.1007/JHEP03(2013)161, arXiv:1212.1456.
- [48] S. El Hedri, A. Hook, M. Jankowiak, and J. G. Wacker, "Learning how to count: A high multiplicity search for the LHC", *JHEP* **08** (2013) 136, doi:10.1007/JHEP08(2013)136, arXiv:1302.1870.
- [49] ATLAS Collaboration, "Search for massive supersymmetric particles decaying to many jets using the ATLAS detector in pp collisions at $\sqrt{s} = 8$ TeV", *Phys. Rev. D* **91** (2015) 112016, doi:10.1103/PhysRevD.91.112016, arXiv:1502.05686.
- [50] ATLAS Collaboration, "Search for new phenomena in final states with large jet multiplicities and missing transverse momentum at $\sqrt{s} = 8$ TeV proton-proton collisions using the ATLAS experiment", *JHEP* **10** (2013) 130, doi:10.1007/JHEP10(2013)130, arXiv:1308.1841. [Erratum: doi:10.1007/JHEP01(2014)109].
- [51] CMS Collaboration, "Commissioning the performance of key observables used in SUSY searches with the first 13 TeV data", CMS Detector Performance Report CMS-DP-2015-035, 2015.
- [52] J. Alwall et al., "The automated computation of tree-level and next-to-leading order differential cross sections, and their matching to parton shower simulations", *JHEP* **07** (2014) 079, doi:10.1007/JHEP07(2014)079, arXiv:1405.0301.
- [53] S. Alioli, P. Nason, C. Oleari, and E. Re, "NLO single-top production matched with shower in POWHEG: s - and t -channel contributions", *JHEP* **09** (2009) 111, doi:10.1088/1126-6708/2009/09/111, arXiv:0907.4076. [Erratum: doi:10.1007/JHEP02(2010)011].

- [54] E. Re, “Single-top Wt-channel production matched with parton showers using the POWHEG method”, *Eur. Phys. J. C* **71** (2011) 1547, doi:10.1140/epjc/s10052-011-1547-z, arXiv:1009.2450.
- [55] NNPDF Collaboration, “Parton distributions for the LHC Run II”, *JHEP* **04** (2015) 040, doi:10.1007/JHEP04(2015)040, arXiv:1410.8849.
- [56] NNPDF Collaboration, “Parton distributions from high-precision collider data”, *Eur. Phys. J. C* **77** (2017) 663, doi:10.1140/epjc/s10052-017-5199-5, arXiv:1706.00428.
- [57] T. Sjöstrand et al., “An Introduction to PYTHIA 8.2”, *Comput. Phys. Commun.* **191** (2015) 159, doi:10.1016/j.cpc.2015.01.024, arXiv:1410.3012.
- [58] CMS Collaboration, “Event generator tunes obtained from underlying event and multiparton scattering measurements”, *Eur. Phys. J. C* **76** (2016) 155, doi:10.1140/epjc/s10052-016-3988-x, arXiv:1512.00815.
- [59] CMS Collaboration, “Extraction and validation of a new set of CMS PYTHIA8 tunes from underlying-event measurements”, (2019). arXiv:1903.12179. Submitted to *Eur. Phys. J. C*.
- [60] GEANT4 Collaboration, “GEANT4 — a simulation toolkit”, *Nucl. Instrum. Meth. A* **506** (2003) 250, doi:10.1016/S0168-9002(03)01368-8.
- [61] CMS Collaboration, “The fast simulation of the CMS detector at LHC”, *J. Phys. Conf. Ser.* **331** (2011) 032049, doi:10.1088/1742-6596/331/3/032049.
- [62] A. Giammanco, “The fast simulation of the CMS experiment”, *J. Phys. Conf. Ser.* **513** (2014) 022012, doi:10.1088/1742-6596/513/2/022012.
- [63] C. Borschensky et al., “Squark and gluino production cross sections in pp collisions at $\sqrt{s} = 13, 14, 33$ and 100 TeV”, *Eur. Phys. J. C* **74** (2014) 3174, doi:10.1140/epjc/s10052-014-3174-y, arXiv:1407.5066.
- [64] W. Beenakker, R. Hopker, M. Spira, and P. M. Zerwas, “Squark and gluino production at hadron colliders”, *Nucl. Phys. B* **492** (1997) 51, doi:10.1016/S0550-3213(97)00084-9, arXiv:hep-ph/9610490.
- [65] A. Kulesza and L. Motyka, “Threshold resummation for squark-antisquark and gluino-pair production at the LHC”, *Phys. Rev. Lett.* **102** (2009) 111802, doi:10.1103/PhysRevLett.102.111802, arXiv:0807.2405.
- [66] A. Kulesza and L. Motyka, “Soft gluon resummation for the production of gluino-gluino and squark-antisquark pairs at the LHC”, *Phys. Rev. D* **80** (2009) 095004, doi:10.1103/PhysRevD.80.095004, arXiv:0905.4749.
- [67] W. Beenakker et al., “Soft-gluon resummation for squark and gluino hadroproduction”, *JHEP* **12** (2009) 041, doi:10.1088/1126-6708/2009/12/041, arXiv:0909.4418.
- [68] W. Beenakker et al., “Squark and gluino hadroproduction”, *Int. J. Mod. Phys. A* **26** (2011) 2637, doi:10.1142/S0217751X11053560, arXiv:1105.1110.
- [69] W. Beenakker et al., “Towards NNLL resummation: hard matching coefficients for squark and gluino hadroproduction”, *JHEP* **10** (2013) 120, doi:10.1007/JHEP10(2013)120, arXiv:1304.6354.

-
- [70] W. Beenakker et al., “NNLL resummation for squark and gluino production at the LHC”, *JHEP* **12** (2014) 023, doi:10.1007/JHEP12(2014)023, arXiv:1404.3134.
- [71] W. Beenakker et al., “NNLL-fast: predictions for coloured supersymmetric particle production at the LHC with threshold and coulomb resummation”, *JHEP* **12** (2016) 133, doi:10.1007/JHEP12(2016)133, arXiv:1607.07741.
- [72] CMS Collaboration, “Search for supersymmetry in proton-proton collisions at 13 tev in final states with jets and missing transverse momentum”, (2019). arXiv:1908.04722. Submitted to *JHEP*.
- [73] CMS Collaboration, “The CMS trigger system”, *JINST* **12** (2017) P01020, doi:10.1088/1748-0221/12/01/P01020, arXiv:1609.02366.
- [74] CMS Collaboration, “The CMS experiment at the CERN LHC”, *JINST* **3** (2008) S08004, doi:10.1088/1748-0221/3/08/S08004.
- [75] CMS Collaboration, “Particle-flow reconstruction and global event description with the CMS detector”, *JINST* **12** (2017) P10003, doi:10.1088/1748-0221/12/10/P10003, arXiv:1706.04965.
- [76] M. Cacciari, G. P. Salam, and G. Soyez, “The anti- k_T jet clustering algorithm”, *JHEP* **04** (2008) 063, doi:10.1088/1126-6708/2008/04/063, arXiv:0802.1189.
- [77] M. Cacciari, G. P. Salam, and G. Soyez, “FastJet user manual”, *Eur. Phys. J. C* **72** (2012) 1896, doi:10.1140/epjc/s10052-012-1896-2, arXiv:1111.6097.
- [78] CMS Collaboration, “Performance of electron reconstruction and selection with the CMS detector in proton-proton collisions at $\sqrt{s} = 8$ TeV”, *JINST* **10** (2015) P06005, doi:10.1088/1748-0221/10/06/P06005, arXiv:1502.02701.
- [79] CMS Collaboration, “Performance of CMS muon reconstruction in pp collision events at $\sqrt{s} = 7$ TeV”, *JINST* **7** (2012) P10002, doi:10.1088/1748-0221/7/10/P10002, arXiv:1206.4071.
- [80] K. Rehermann and B. Tweedie, “Efficient identification of boosted semileptonic top quarks at the LHC”, *JHEP* **03** (2011) 059, doi:10.1007/JHEP03(2011)059, arXiv:1007.2221.
- [81] CMS Collaboration, “Determination of jet energy calibration and transverse momentum resolution in CMS”, *JINST* **6** (2011) P11002, doi:10.1088/1748-0221/6/11/P11002, arXiv:1107.4277.
- [82] M. Cacciari and G. P. Salam, “Pileup subtraction using jet areas”, *Phys. Lett. B* **659** (2008) 119, doi:10.1016/j.physletb.2007.09.077, arXiv:0707.1378.
- [83] CMS Collaboration, “Identification of heavy-flavour jets with the CMS detector in pp collisions at 13 tev”, *JINST* **13** (2018) P05011, doi:10.1088/1748-0221/13/05/P05011, arXiv:1712.07158.
- [84] CMS Collaboration, “Jet energy scale and resolution in the cms experiment in pp collisions at 8 TeV”, *JINST* **12** (2017) P02014, doi:10.1088/1748-0221/12/02/P02014, arXiv:1607.03663.

- [85] CMS Collaboration, “Performance of missing transverse momentum in pp collisions at $\sqrt{s} = 13$ TeV using the CMS detector”, CMS Physics Analysis Summary CMS-PAS-JME-17-001, 2018.
- [86] C. G. Lester and D. J. Summers, “Measuring masses of semi-invisibly decaying particle pairs produced at hadron colliders”, *Phys. Lett. B* **463** (1999) 5, doi:10.1016/S0370-2693(99)00945-4, arXiv:hep-ph/9906349.
- [87] A. Barr, C. Lester, and P. Stephens, “A variable for measuring masses at hadron colliders when missing energy is expected; m_{T2} : the truth behind the glamour”, *J. Phys. G* **29** (2003) 2343, doi:10.1088/0954-3899/29/10/304, arXiv:hep-ph/0304226.
- [88] CMS Collaboration, “CMS luminosity measurement for the 2016 data-taking period at $\sqrt{s} = 13$ TeV”, CMS Physics Analysis Summary CMS-PAS-LUM-17-001, 2017.
- [89] CMS Collaboration, “CMS luminosity measurement for the 2017 data-taking period at $\sqrt{s} = 13$ TeV”, CMS Physics Analysis Summary CMS-PAS-LUM-17-004, 2018.
- [90] CMS Collaboration, “CMS luminosity measurement for the 2018 data-taking period at $\sqrt{s} = 13$ TeV”, CMS Physics Analysis Summary CMS-PAS-LUM-18-002, 2019.
- [91] T. Junk, “Confidence level computation for combining searches with small statistics”, *Nucl. Instrum. Meth. A* **434** (1999) 435, doi:10.1016/S0168-9002(99)00498-2, arXiv:hep-ex/9902006.
- [92] A. L. Read, “Presentation of search results: the CL_s technique”, in *Durham IPPP Workshop: Advanced Statistical Techniques in Particle Physics*, p. 2693. Durham, UK, March, 2002. [*J. Phys. G* **28** (2002) 2693]. doi:10.1088/0954-3899/28/10/313.
- [93] ATLAS and CMS Collaborations, LHC Higgs Combination Group, “Procedure for the LHC Higgs boson search combination in Summer 2011”, Technical Report CMS-NOTE-2011-005, ATL-PHYS-PUB-2011-11, 2011.
- [94] G. Cowan, K. Cranmer, E. Gross, and O. Vitells, “Asymptotic formulae for likelihood-based tests of new physics”, *Eur. Phys. J. C* **71** (2011) 1554, doi:10.1140/epjc/s10052-011-1554-0, arXiv:1007.1727. [Erratum: doi:10.1140/epjc/s10052-013-2501-z].
- [95] CMS Collaboration, “Search for the pair production of light top squarks in the $e^\pm\mu^\mp$ final state in proton-proton collisions at $\sqrt{s} = 13$ TeV”, *JHEP* **03** (2019) 101, doi:10.1007/JHEP03(2019)101, arXiv:1901.01288.

A The CMS Collaboration

Yerevan Physics Institute, Yerevan, Armenia

A.M. Sirunyan[†], A. Tumasyan

Institut für Hochenergiephysik, Wien, Austria

W. Adam, F. Ambrogi, T. Bergauer, M. Dragicevic, J. Erö, A. Escalante Del Valle, M. Flechl, R. Frühwirth¹, M. Jeitler¹, N. Krammer, I. Krätschmer, D. Liko, T. Madlener, I. Mikulec, N. Rad, J. Schieck¹, R. Schöfbeck, M. Spanring, W. Waltenberger, C.-E. Wulz¹, M. Zarucki

Institute for Nuclear Problems, Minsk, Belarus

V. Drugakov, V. Mossolov, J. Suarez Gonzalez

Universiteit Antwerpen, Antwerpen, Belgium

M.R. Darwish, E.A. De Wolf, D. Di Croce, X. Janssen, A. Lelek, M. Pieters, H. Rejeb Sfar, H. Van Haevermaet, P. Van Mechelen, S. Van Putte, N. Van Remortel

Vrije Universiteit Brussel, Brussel, Belgium

F. Blekman, E.S. Bols, S.S. Chhibra, J. D'Hondt, J. De Clercq, D. Lontkovskyi, S. Lowette, I. Marchesini, S. Moortgat, Q. Python, K. Skovpen, S. Tavernier, W. Van Doninck, P. Van Mulders

Université Libre de Bruxelles, Bruxelles, Belgium

D. Beghin, B. Bilin, B. Clerbaux, G. De Lentdecker, H. Delannoy, B. Dorney, L. Favart, A. Grebenyuk, A.K. Kalsi, L. Moureaux, A. Popov, N. Postiau, E. Starling, L. Thomas, C. Vander Velde, P. Vanlaer, D. Vannerom

Ghent University, Ghent, Belgium

T. Cornelis, D. Dobur, I. Khvastunov², M. Niedziela, C. Roskas, M. Tytgat, W. Verbeke, B. Vermassen, M. Vit

Université Catholique de Louvain, Louvain-la-Neuve, Belgium

O. Bondu, G. Bruno, C. Caputo, P. David, C. Delaere, M. Delcourt, A. Giammanco, V. Lemaitre, J. Prisciandaro, A. Saggio, M. Vidal Marono, P. Vischia, J. Zobec

Centro Brasileiro de Pesquisas Físicas, Rio de Janeiro, Brazil

F.L. Alves, G.A. Alves, G. Correia Silva, C. Hensel, A. Moraes, P. Rebello Teles

Universidade do Estado do Rio de Janeiro, Rio de Janeiro, Brazil

E. Belchior Batista Das Chagas, W. Carvalho, J. Chinellato³, E. Coelho, E.M. Da Costa, G.G. Da Silveira⁴, D. De Jesus Damiao, C. De Oliveira Martins, S. Fonseca De Souza, L.M. Huertas Guativa, H. Malbouisson, J. Martins⁵, D. Matos Figueiredo, M. Medina Jaime⁶, M. Melo De Almeida, C. Mora Herrera, L. Mundim, H. Nogima, W.L. Prado Da Silva, L.J. Sanchez Rosas, A. Santoro, A. Sznajder, M. Thiel, E.J. Tonelli Manganote³, F. Torres Da Silva De Araujo, A. Vilela Pereira

Universidade Estadual Paulista ^a, Universidade Federal do ABC ^b, São Paulo, Brazil

C.A. Bernardes^a, L. Calligaris^a, T.R. Fernandez Perez Tomei^a, E.M. Gregores^b, D.S. Lemos, P.G. Mercadante^b, S.F. Novaes^a, SandraS. Padula^a

Institute for Nuclear Research and Nuclear Energy, Bulgarian Academy of Sciences, Sofia, Bulgaria

A. Aleksandrov, G. Antchev, R. Hadjiiska, P. Iaydjiev, M. Misheva, M. Rodozov, M. Shopova, G. Sultanov

University of Sofia, Sofia, Bulgaria

M. Bonchev, A. Dimitrov, T. Ivanov, L. Litov, B. Pavlov, P. Petkov, A. Petrov

Beihang University, Beijing, China

W. Fang⁷, X. Gao⁷, L. Yuan

Department of Physics, Tsinghua University, Beijing, China

M. Ahmad, Z. Hu, Y. Wang

Institute of High Energy Physics, Beijing, China

G.M. Chen⁸, H.S. Chen⁸, M. Chen, C.H. Jiang, D. Leggat, H. Liao, Z. Liu, A. Spiezia, J. Tao, E. Yazgan, H. Zhang, S. Zhang⁸, J. Zhao

State Key Laboratory of Nuclear Physics and Technology, Peking University, Beijing, China

A. Agapitos, Y. Ban, G. Chen, A. Levin, J. Li, L. Li, Q. Li, Y. Mao, S.J. Qian, D. Wang, Q. Wang

Zhejiang University, Hangzhou, China

M. Xiao

Universidad de Los Andes, Bogota, Colombia

C. Avila, A. Cabrera, C. Florez, C.F. González Hernández, M.A. Segura Delgado

Universidad de Antioquia, Medellin, Colombia

J. Mejia Guisao, J.D. Ruiz Alvarez, C.A. Salazar González, N. Vanegas Arbelaez

University of Split, Faculty of Electrical Engineering, Mechanical Engineering and Naval Architecture, Split, Croatia

D. Giljanović, N. Godinovic, D. Lelas, I. Puljak, T. Sculac

University of Split, Faculty of Science, Split, Croatia

Z. Antunovic, M. Kovac

Institute Rudjer Boskovic, Zagreb, Croatia

V. Brigljevic, D. Ferencek, K. Kadija, B. Mesic, M. Roguljic, A. Starodumov⁹, T. Susa

University of Cyprus, Nicosia, Cyprus

M.W. Ather, A. Attikis, E. Erodotou, A. Ioannou, M. Kolosova, S. Konstantinou, G. Mavromanolakis, J. Mousa, C. Nicolaou, F. Ptochos, P.A. Razis, H. Rykaczewski, D. Tsiakkouri

Charles University, Prague, Czech Republic

M. Finger¹⁰, M. Finger Jr.¹⁰, A. Kveton, J. Tomsa

Escuela Politecnica Nacional, Quito, Ecuador

E. Ayala

Universidad San Francisco de Quito, Quito, Ecuador

E. Carrera Jarrin

Academy of Scientific Research and Technology of the Arab Republic of Egypt, Egyptian Network of High Energy Physics, Cairo, Egypt

H. Abdalla¹¹, S. Khalil¹²

National Institute of Chemical Physics and Biophysics, Tallinn, Estonia

S. Bhowmik, A. Carvalho Antunes De Oliveira, R.K. Dewanjee, K. Ehataht, M. Kadastik, M. Raidal, C. Veelken

Department of Physics, University of Helsinki, Helsinki, Finland

P. Eerola, L. Forthomme, H. Kirschenmann, K. Osterberg, M. Voutilainen

Helsinki Institute of Physics, Helsinki, Finland

F. Garcia, J. Havukainen, J.K. Heikkilä, V. Karimäki, M.S. Kim, R. Kinnunen, T. Lampén, K. Lassila-Perini, S. Laurila, S. Lehti, T. Lindén, P. Luukka, T. Mäenpää, H. Siikonen, E. Tuominen, J. Tuominiemi

Lappeenranta University of Technology, Lappeenranta, Finland

T. Tuuva

IRFU, CEA, Université Paris-Saclay, Gif-sur-Yvette, France

M. Besancon, F. Couderc, M. Dejardin, D. Denegri, B. Fabbro, J.L. Faure, F. Ferri, S. Ganjour, A. Givernaud, P. Gras, G. Hamel de Monchenault, P. Jarry, C. Leloup, B. Lenzi, E. Locci, J. Malcles, J. Rander, A. Rosowsky, M.Ö. Sahin, A. Savoy-Navarro¹³, M. Titov, G.B. Yu

Laboratoire Leprince-Ringuet, CNRS/IN2P3, Ecole Polytechnique, Institut Polytechnique de Paris

S. Ahuja, C. Amendola, F. Beaudette, P. Busson, C. Charlot, B. Diab, G. Falmagne, R. Granier de Cassagnac, I. Kucher, A. Lobanov, C. Martin Perez, M. Nguyen, C. Ochando, P. Paganini, J. Rembser, R. Salerno, J.B. Sauvan, Y. Sirois, A. Zabi, A. Zghiche

Université de Strasbourg, CNRS, IPHC UMR 7178, Strasbourg, France

J.-L. Agram¹⁴, J. Andrea, D. Bloch, G. Bourgatte, J.-M. Brom, E.C. Chabert, C. Collard, E. Conte¹⁴, J.-C. Fontaine¹⁴, D. Gelé, U. Goerlach, M. Jansová, A.-C. Le Bihan, N. Tonon, P. Van Hove

Centre de Calcul de l'Institut National de Physique Nucleaire et de Physique des Particules, CNRS/IN2P3, Villeurbanne, France

S. Gadrat

Université de Lyon, Université Claude Bernard Lyon 1, CNRS-IN2P3, Institut de Physique Nucléaire de Lyon, Villeurbanne, France

S. Beauceron, C. Bernet, G. Boudoul, C. Camen, A. Carle, N. Chanon, R. Chierici, D. Contardo, P. Depasse, H. El Mamouni, J. Fay, S. Gascon, M. Gouzevitch, B. Ille, Sa. Jain, F. Lagarde, I.B. Laktineh, H. Lattaud, A. Lesauvage, M. Lethuillier, L. Mirabito, S. Perries, V. Sordini, L. Torterotot, G. Touquet, M. Vander Donckt, S. Viret

Georgian Technical University, Tbilisi, Georgia

A. Khvedelidze¹⁰

Tbilisi State University, Tbilisi, Georgia

Z. Tsamalaidze¹⁰

RWTH Aachen University, I. Physikalisches Institut, Aachen, Germany

C. Autermann, L. Feld, K. Klein, M. Lipinski, D. Meuser, A. Pauls, M. Preuten, M.P. Rauch, J. Schulz, M. Teroerde, B. Wittmer

RWTH Aachen University, III. Physikalisches Institut A, Aachen, Germany

M. Erdmann, B. Fischer, S. Ghosh, T. Hebbeker, K. Hoepfner, H. Keller, L. Mastrolorenzo, M. Merschmeyer, A. Meyer, P. Millet, G. Mocellin, S. Mondal, S. Mukherjee, D. Noll, A. Novak, T. Pook, A. Pozdnyakov, T. Quast, M. Radziej, Y. Rath, H. Reithler, J. Roemer, A. Schmidt, S.C. Schuler, A. Sharma, S. Wiedenbeck, S. Zaleski

RWTH Aachen University, III. Physikalisches Institut B, Aachen, Germany

G. Flügge, W. Haj Ahmad¹⁵, O. Hlushchenko, T. Kress, T. Müller, A. Nowack, C. Pistone, O. Pooth, D. Roy, H. Sert, A. Stahl¹⁶

Deutsches Elektronen-Synchrotron, Hamburg, Germany

M. Aldaya Martin, P. Asmuss, I. Babounikau, H. Bakhshiansohi, K. Beernaert, O. Behnke, A. Bermúdez Martínez, D. Bertsche, A.A. Bin Anuar, K. Borras¹⁷, V. Botta, A. Campbell, A. Cardini, P. Connor, S. Consuegra Rodríguez, C. Contreras-Campana, V. Danilov, A. De Wit, M.M. Defranchis, C. Diez Pardos, D. Domínguez Damiani, G. Eckerlin, D. Eckstein, T. Eichhorn, A. Elwood, E. Eren, E. Gallo¹⁸, A. Geiser, A. Grohsjean, M. Guthoff, M. Haranko, A. Harb, A. Jafari, N.Z. Jomhari, H. Jung, A. Kasem¹⁷, M. Kasemann, H. Kaveh, J. Keaveney, C. Kleinwort, J. Knolle, D. Krücker, W. Lange, T. Lenz, J. Lidrych, K. Lipka, W. Lohmann¹⁹, R. Mankel, I.-A. Melzer-Pellmann, A.B. Meyer, M. Meyer, M. Missiroli, J. Mnich, A. Mussgiller, V. Myronenko, D. Pérez Adán, S.K. Pflitsch, D. Pitzl, A. Raspereza, A. Saibel, M. Savitskyi, V. Scheurer, P. Schütze, C. Schwanenberger, R. Shevchenko, A. Singh, H. Tholen, O. Turkot, A. Vagnerini, M. Van De Klundert, R. Walsh, Y. Wen, K. Wichmann, C. Wissing, O. Zenaiev, R. Zlebcik

University of Hamburg, Hamburg, Germany

R. Aggleton, S. Bein, L. Benato, A. Benecke, V. Blobel, T. Dreyer, A. Ebrahimi, F. Feindt, A. Fröhlich, C. Garbers, E. Garutti, D. Gonzalez, P. Gunnellini, J. Haller, A. Hinzmann, A. Karavdina, G. Kasieczka, R. Klanner, R. Kogler, N. Kovalchuk, S. Kurz, V. Kutzner, J. Lange, T. Lange, A. Malara, J. Multhaupt, C.E.N. Niemeyer, A. Perieanu, A. Reimers, O. Rieger, C. Scharf, P. Schleper, S. Schumann, J. Schwandt, J. Sonneveld, H. Stadie, G. Steinbrück, F.M. Stober, B. Vormwald, I. Zoi

Karlsruher Institut fuer Technologie, Karlsruhe, Germany

M. Akbiyik, C. Barth, M. Baselga, S. Baur, T. Berger, E. Butz, R. Caspart, T. Chwalek, W. De Boer, A. Dierlamm, K. El Morabit, N. Faltermann, M. Giffels, P. Goldenzweig, A. Gottmann, M.A. Harrendorf, F. Hartmann¹⁶, U. Husemann, S. Kudella, S. Mitra, M.U. Mozer, D. Müller, Th. Müller, M. Musich, A. Nürnberg, G. Quast, K. Rabbertz, M. Schröder, I. Shvetsov, H.J. Simonis, R. Ulrich, M. Wassmer, M. Weber, C. Wöhrmann, R. Wolf

Institute of Nuclear and Particle Physics (INPP), NCSR Demokritos, Aghia Paraskevi, Greece

G. Anagnostou, P. Asenov, G. Daskalakis, T. Geralis, A. Kyriakis, D. Loukas, G. Paspalaki

National and Kapodistrian University of Athens, Athens, Greece

M. Diamantopoulou, G. Karathanasis, P. Kontaxakis, A. Manousakis-katsikakis, A. Panagiotou, I. Papavergou, N. Saoulidou, A. Stakia, K. Theofilatos, K. Vellidis, E. Vourliotis

National Technical University of Athens, Athens, Greece

G. Bakas, K. Kousouris, I. Papakrivopoulos, G. Tsipolitis

University of Ioánnina, Ioánnina, Greece

I. Evangelou, C. Foudas, P. Giannelis, P. Katsoulis, P. Kokkas, S. Mallios, K. Manitaras, N. Manthos, I. Papadopoulos, J. Strologas, F.A. Triantis, D. Tsitsonis

MTA-ELTE Lendület CMS Particle and Nuclear Physics Group, Eötvös Loránd University, Budapest, Hungary

M. Bartók²⁰, R. Chudasama, M. Csanad, P. Major, K. Mandal, A. Mehta, M.I. Nagy, G. Pasztor, O. Surányi, G.I. Veres

Wigner Research Centre for Physics, Budapest, Hungary

G. Bencze, C. Hajdu, D. Horvath²¹, F. Sikler, T.Á. Vámi, V. Veszpremi, G. Vesztergombi[†]

Institute of Nuclear Research ATOMKI, Debrecen, Hungary

N. Beni, S. Czellar, J. Karancsi²⁰, J. Molnar, Z. Szillasi

Institute of Physics, University of Debrecen, Debrecen, Hungary

P. Raics, D. Teyssier, Z.L. Trocsanyi, B. Ujvari

Eszterhazy Karoly University, Karoly Robert Campus, Gyongyos, Hungary

T. Csorgo, W.J. Metzger, F. Nemes, T. Novak

Indian Institute of Science (IISc), Bangalore, India

S. Choudhury, J.R. Komaragiri, P.C. Tiwari

National Institute of Science Education and Research, HBNI, Bhubaneswar, IndiaS. Bahinipati²³, C. Kar, G. Kole, P. Mal, V.K. Muraleedharan Nair Bindhu, A. Nayak²⁴, D.K. Sahoo²³, S.K. Swain**Panjab University, Chandigarh, India**

S. Bansal, S.B. Beri, V. Bhatnagar, S. Chauhan, N. Dhingra, R. Gupta, A. Kaur, M. Kaur, S. Kaur, P. Kumari, M. Lohan, M. Meena, K. Sandeep, S. Sharma, J.B. Singh, A.K. Viridi

University of Delhi, Delhi, India

A. Bhardwaj, B.C. Choudhary, R.B. Garg, M. Gola, S. Keshri, Ashok Kumar, M. Naimuddin, P. Priyanka, K. Ranjan, Aashaq Shah, R. Sharma

Saha Institute of Nuclear Physics, HBNI, Kolkata, IndiaR. Bhardwaj²⁵, M. Bharti²⁵, R. Bhattacharya, S. Bhattacharya, U. Bhawandeep²⁵, D. Bhowmik, S. Dutta, S. Ghosh, B. Gomber²⁶, M. Maity²⁷, K. Mondal, S. Nandan, A. Purohit, P.K. Rout, G. Saha, S. Sarkar, T. Sarkar²⁷, M. Sharan, B. Singh²⁵, S. Thakur²⁵**Indian Institute of Technology Madras, Madras, India**

P.K. Behera, P. Kalbhor, A. Muhammad, P.R. Pujahari, A. Sharma, A.K. Sikdar

Bhabha Atomic Research Centre, Mumbai, India

D. Dutta, V. Jha, V. Kumar, D.K. Mishra, P.K. Netrakanti, L.M. Pant, P. Shukla

Tata Institute of Fundamental Research-A, Mumbai, India

T. Aziz, M.A. Bhat, S. Dugad, G.B. Mohanty, N. Sur, RavindraKumar Verma

Tata Institute of Fundamental Research-B, Mumbai, India

S. Banerjee, S. Bhattacharya, S. Chatterjee, P. Das, M. Guchait, S. Karmakar, S. Kumar, G. Majumder, K. Mazumdar, N. Sahoo, S. Sawant

Indian Institute of Science Education and Research (IISER), Pune, India

S. Dube, B. Kansal, A. Kapoor, K. Kothekar, S. Pandey, A. Rane, A. Rastogi, S. Sharma

Institute for Research in Fundamental Sciences (IPM), Tehran, IranS. Chenarani²⁸, E. Eskandari Tadavani, S.M. Etesami²⁸, M. Khakzad, M. Mohammadi Najafabadi, M. Naseri, F. Rezaei Hosseinabadi**University College Dublin, Dublin, Ireland**

M. Felcini, M. Grunewald

INFN Sezione di Bari ^a, Università di Bari ^b, Politecnico di Bari ^c, Bari, ItalyM. Abbrescia^{a,b}, R. Aly^{a,b,29}, C. Calabria^{a,b}, A. Colaleo^a, D. Creanza^{a,c}, L. Cristella^{a,b}, N. De Filippis^{a,c}, M. De Palma^{a,b}, A. Di Florio^{a,b}, W. Elmetenawee^{a,b}, L. Fiore^a, A. Gelmi^{a,b}, G. Iaselli^{a,c}, M. Ince^{a,b}, S. Lezki^{a,b}, G. Maggi^{a,c}, M. Maggi^a, J.A. Merlin, G. Miniello^{a,b}, S. My^{a,b}, S. Nuzzo^{a,b}, A. Pompili^{a,b}, G. Pugliese^{a,c}, R. Radogna^a, A. Ranieri^a, G. Selvaggi^{a,b}, L. Silvestris^a, F.M. Simone^{a,b}, R. Venditti^a, P. Verwilligen^a

INFN Sezione di Bologna ^a, Università di Bologna ^b, Bologna, Italy

G. Abbiendi^a, C. Battilana^{a,b}, D. Bonacorsi^{a,b}, L. Borgonovi^{a,b}, S. Braibant-Giacomelli^{a,b}, R. Campanini^{a,b}, P. Capiluppi^{a,b}, A. Castro^{a,b}, F.R. Cavallo^a, C. Ciocca^a, G. Codispoti^{a,b}, M. Cuffiani^{a,b}, G.M. Dallavalle^a, F. Fabbri^a, A. Fanfani^{a,b}, E. Fontanesi^{a,b}, P. Giacomelli^a, C. Grandi^a, L. Guiducci^{a,b}, F. Iemmi^{a,b}, S. Lo Meo^{a,30}, S. Marcellini^a, G. Masetti^a, F.L. Navarria^{a,b}, A. Perrotta^a, F. Primavera^{a,b}, A.M. Rossi^{a,b}, T. Rovelli^{a,b}, G.P. Siroli^{a,b}, N. Tosi^a

INFN Sezione di Catania ^a, Università di Catania ^b, Catania, Italy

S. Albergo^{a,b,31}, S. Costa^{a,b}, A. Di Mattia^a, R. Potenza^{a,b}, A. Tricomi^{a,b,31}, C. Tuve^{a,b}

INFN Sezione di Firenze ^a, Università di Firenze ^b, Firenze, Italy

G. Barbagli^a, A. Cassese, R. Ceccarelli, V. Ciulli^{a,b}, C. Civinini^a, R. D'Alessandro^{a,b}, F. Fiori^{a,c}, E. Focardi^{a,b}, G. Latino^{a,b}, P. Lenzi^{a,b}, M. Meschini^a, S. Paoletti^a, G. Sguazzoni^a, L. Viliani^a

INFN Laboratori Nazionali di Frascati, Frascati, Italy

L. Benussi, S. Bianco, D. Piccolo

INFN Sezione di Genova ^a, Università di Genova ^b, Genova, Italy

M. Bozzo^{a,b}, F. Ferro^a, R. Mulargia^{a,b}, E. Robutti^a, S. Tosi^{a,b}

INFN Sezione di Milano-Bicocca ^a, Università di Milano-Bicocca ^b, Milano, Italy

A. Benaglia^a, A. Beschi^{a,b}, F. Brivio^{a,b}, V. Ciriolo^{a,b,16}, M.E. Dinardo^{a,b}, P. Dini^a, S. Gennai^a, A. Ghezzi^{a,b}, P. Govoni^{a,b}, L. Guzzi^{a,b}, M. Malberti^a, S. Malvezzi^a, D. Menasce^a, F. Monti^{a,b}, L. Moroni^a, M. Paganoni^{a,b}, D. Pedrini^a, S. Ragazzi^{a,b}, T. Tabarelli de Fatis^{a,b}, D. Valsecchi^{a,b}, D. Zuolo^{a,b}

INFN Sezione di Napoli ^a, Università di Napoli 'Federico II' ^b, Napoli, Italy, Università della Basilicata ^c, Potenza, Italy, Università G. Marconi ^d, Roma, Italy

S. Buontempo^a, N. Cavallo^{a,c}, A. De Iorio^{a,b}, A. Di Crescenzo^{a,b}, F. Fabozzi^{a,c}, F. Fienga^a, G. Galati^a, A.O.M. Iorio^{a,b}, L. Lista^{a,b}, S. Meola^{a,d,16}, P. Paolucci^{a,16}, B. Rossi^a, C. Sciacca^{a,b}, E. Voevodina^{a,b}

INFN Sezione di Padova ^a, Università di Padova ^b, Padova, Italy, Università di Trento ^c, Trento, Italy

P. Azzi^a, N. Bacchetta^a, D. Bisello^{a,b}, A. Boletti^{a,b}, A. Bragagnolo^{a,b}, R. Carlin^{a,b}, P. Checchia^a, P. De Castro Manzano^a, T. Dorigo^a, U. Dosselli^a, F. Gasparini^{a,b}, U. Gasparini^{a,b}, A. Gozzelino^a, S.Y. Hoh^{a,b}, P. Lujan^a, M. Margoni^{a,b}, A.T. Meneguzzo^{a,b}, J. Pazzini^{a,b}, M. Presilla^b, P. Ronchese^{a,b}, R. Rossin^{a,b}, F. Simonetto^{a,b}, A. Tiko^a, M. Tosi^{a,b}, M. Zanetti^{a,b}, P. Zotto^{a,b}, G. Zumerle^{a,b}

INFN Sezione di Pavia ^a, Università di Pavia ^b, Pavia, Italy

A. Braghieri^a, D. Fiorina^{a,b}, P. Montagna^{a,b}, S.P. Ratti^{a,b}, V. Re^a, M. Ressegotti^{a,b}, C. Riccardi^{a,b}, P. Salvini^a, I. Vai^a, P. Vitulo^{a,b}

INFN Sezione di Perugia ^a, Università di Perugia ^b, Perugia, Italy

M. Biasini^{a,b}, G.M. Bilei^a, D. Ciangottini^{a,b}, L. Fanò^{a,b}, P. Lariccia^{a,b}, R. Leonardi^{a,b}, E. Manoni^a, G. Mantovani^{a,b}, V. Mariani^{a,b}, M. Menichelli^a, A. Rossi^{a,b}, A. Santocchia^{a,b}, D. Spiga^a

INFN Sezione di Pisa ^a, Università di Pisa ^b, Scuola Normale Superiore di Pisa ^c, Pisa, Italy

K. Androsov^a, P. Azzurri^a, G. Bagliesi^a, V. Bertacchi^{a,c}, L. Bianchini^a, T. Boccali^a, R. Castaldi^a, M.A. Ciocci^{a,b}, R. Dell'Orso^a, S. Donato^a, G. Fedi^a, L. Giannini^{a,c}, A. Giassi^a, M.T. Grippo^a, F. Ligabue^{a,c}, E. Manca^{a,c}, G. Mandorli^{a,c}, A. Messineo^{a,b}, F. Palla^a, A. Rizzi^{a,b}, G. Rolandi³², S. Roy Chowdhury, A. Scribano^a, P. Spagnolo^a, R. Tenchini^a, G. Tonelli^{a,b}, N. Turini, A. Venturi^a, P.G. Verdini^a

INFN Sezione di Roma ^a, Sapienza Università di Roma ^b, Rome, Italy

F. Cavallari^a, M. Cipriani^{a,b}, D. Del Re^{a,b}, E. Di Marco^a, M. Diemoz^a, E. Longo^{a,b}, P. Meridiani^a, G. Organtini^{a,b}, F. Pandolfi^a, R. Paramatti^{a,b}, C. Quaranta^{a,b}, S. Rahatlou^{a,b}, C. Rovelli^a, F. Santanastasio^{a,b}, L. Soffi^{a,b}

INFN Sezione di Torino ^a, Università di Torino ^b, Torino, Italy, Università del Piemonte Orientale ^c, Novara, Italy

N. Amapane^{a,b}, R. Arcidiacono^{a,c}, S. Argiro^{a,b}, M. Arneodo^{a,c}, N. Bartosik^a, R. Bellan^{a,b}, A. Bellora, C. Biino^a, A. Cappati^{a,b}, N. Cartiglia^a, S. Cometti^a, M. Costa^{a,b}, R. Covarelli^{a,b}, N. Demaria^a, B. Kiani^{a,b}, F. Legger, C. Mariotti^a, S. Maselli^a, E. Migliore^{a,b}, V. Monaco^{a,b}, E. Monteil^{a,b}, M. Monteno^a, M.M. Obertino^{a,b}, G. Ortona^{a,b}, L. Pacher^{a,b}, N. Pastrone^a, M. Pelliccioni^a, G.L. Pinna Angioni^{a,b}, A. Romero^{a,b}, M. Ruspa^{a,c}, R. Salvatico^{a,b}, V. Sola^a, A. Solano^{a,b}, D. Soldi^{a,b}, A. Staiano^a, D. Trocino^{a,b}

INFN Sezione di Trieste ^a, Università di Trieste ^b, Trieste, Italy

S. Belforte^a, V. Candelise^{a,b}, M. Casarsa^a, F. Cossutti^a, A. Da Rold^{a,b}, G. Della Ricca^{a,b}, F. Vazzoler^{a,b}, A. Zanetti^a

Kyungpook National University, Daegu, Korea

B. Kim, D.H. Kim, G.N. Kim, J. Lee, S.W. Lee, C.S. Moon, Y.D. Oh, S.I. Pak, S. Sekmen, D.C. Son, Y.C. Yang

Chonnam National University, Institute for Universe and Elementary Particles, Kwangju, Korea

H. Kim, D.H. Moon, G. Oh

Hanyang University, Seoul, Korea

B. Francois, T.J. Kim, J. Park

Korea University, Seoul, Korea

S. Cho, S. Choi, Y. Go, S. Ha, B. Hong, K. Lee, K.S. Lee, J. Lim, J. Park, S.K. Park, Y. Roh, J. Yoo

Kyung Hee University, Department of Physics

J. Goh

Sejong University, Seoul, Korea

H.S. Kim

Seoul National University, Seoul, Korea

J. Almond, J.H. Bhyun, J. Choi, S. Jeon, J. Kim, J.S. Kim, H. Lee, K. Lee, S. Lee, K. Nam, M. Oh, S.B. Oh, B.C. Radburn-Smith, U.K. Yang, H.D. Yoo, I. Yoon

University of Seoul, Seoul, Korea

D. Jeon, J.H. Kim, J.S.H. Lee, I.C. Park, I.J. Watson

Sungkyunkwan University, Suwon, Korea

Y. Choi, C. Hwang, Y. Jeong, J. Lee, Y. Lee, I. Yu

Riga Technical University, Riga, Latvia

V. Veckalns³³

Vilnius University, Vilnius, Lithuania

V. Dudenas, A. Juodagalvis, A. Rinkevicius, G. Tamulaitis, J. Vaitkus

National Centre for Particle Physics, Universiti Malaya, Kuala Lumpur, Malaysia

Z.A. Ibrahim, F. Mohamad Idris³⁴, W.A.T. Wan Abdullah, M.N. Yusli, Z. Zolkapli

Universidad de Sonora (UNISON), Hermosillo, Mexico

J.F. Benitez, A. Castaneda Hernandez, J.A. Murillo Quijada, L. Valencia Palomo

Centro de Investigacion y de Estudios Avanzados del IPN, Mexico City, Mexico

H. Castilla-Valdez, E. De La Cruz-Burelo, I. Heredia-De La Cruz³⁵, R. Lopez-Fernandez, A. Sanchez-Hernandez

Universidad Iberoamericana, Mexico City, Mexico

S. Carrillo Moreno, C. Oropeza Barrera, M. Ramirez-Garcia, F. Vazquez Valencia

Benemerita Universidad Autonoma de Puebla, Puebla, Mexico

J. Eysermans, I. Pedraza, H.A. Salazar Ibarguen, C. Uribe Estrada

Universidad Autónoma de San Luis Potosí, San Luis Potosí, Mexico

A. Morelos Pineda

University of Montenegro, Podgorica, Montenegro

J. Mijuskovic², N. Raicevic

University of Auckland, Auckland, New Zealand

D. Krofcheck

University of Canterbury, Christchurch, New Zealand

S. Bheesette, P.H. Butler

National Centre for Physics, Quaid-I-Azam University, Islamabad, Pakistan

A. Ahmad, M. Ahmad, Q. Hassan, H.R. Hoorani, W.A. Khan, M.A. Shah, M. Shoaib, M. Waqas

AGH University of Science and Technology Faculty of Computer Science, Electronics and Telecommunications, Krakow, Poland

V. Avati, L. Grzanka, M. Malawski

National Centre for Nuclear Research, Swierk, Poland

H. Bialkowska, M. Bluj, B. Boimska, M. Górski, M. Kazana, M. Szeleper, P. Zalewski

Institute of Experimental Physics, Faculty of Physics, University of Warsaw, Warsaw, Poland

K. Bunkowski, A. Byszuk³⁶, K. Doroba, A. Kalinowski, M. Konecki, J. Krolikowski, M. Olszewski, M. Walczak

Laboratório de Instrumentação e Física Experimental de Partículas, Lisboa, Portugal

M. Araujo, P. Bargassa, D. Bastos, A. Di Francesco, P. Faccioli, B. Galinhas, M. Gallinaro, J. Hollar, N. Leonardo, T. Niknejad, J. Seixas, K. Shchelina, G. Strong, O. Toldaiev, J. Varela

Joint Institute for Nuclear Research, Dubna, Russia

S. Afanasiev, P. Bunin, M. Gavrilenko, I. Golutvin, I. Gorbunov, A. Kamenev, V. Karjavine, A. Lanev, A. Malakhov, V. Matveev^{37,38}, P. Moiseenz, V. Palichik, V. Perelygin, M. Savina, S. Shmatov, S. Shulha, N. Skatchkov, V. Smirnov, N. Voytishin, A. Zarubin

Petersburg Nuclear Physics Institute, Gatchina (St. Petersburg), Russia

L. Chtchipounov, V. Golovtcov, Y. Ivanov, V. Kim³⁹, E. Kuznetsova⁴⁰, P. Levchenko, V. Murzin, V. Oreshkin, I. Smirnov, D. Sosnov, V. Sulimov, L. Uvarov, A. Vorobyev

Institute for Nuclear Research, Moscow, Russia

Yu. Andreev, A. Dermenev, S. Gninenko, N. Golubev, A. Karneyeu, M. Kirsanov, N. Krasnikov, A. Pashenkov, D. Tlisov, A. Toropin

Institute for Theoretical and Experimental Physics named by A.I. Alikhanov of NRC 'Kurchatov Institute', Moscow, Russia

V. Epshteyn, V. Gavrilov, N. Lychkovskaya, A. Nikitenko⁴¹, V. Popov, I. Pozdnyakov, G. Safronov, A. Spiridonov, A. Stepenov, M. Toms, E. Vlasov, A. Zhokin

Moscow Institute of Physics and Technology, Moscow, Russia

T. Aushev

National Research Nuclear University 'Moscow Engineering Physics Institute' (MEPhI), Moscow, Russia

M. Danilov⁴², D. Philippov, S. Polikarpov⁴², E. Tarkovskii, E. Zhemchugov

P.N. Lebedev Physical Institute, Moscow, Russia

V. Andreev, M. Azarkin, I. Dremin, M. Kirakosyan, A. Terkulov

Skobeltsyn Institute of Nuclear Physics, Lomonosov Moscow State University, Moscow, Russia

A. Baskakov, A. Belyaev, E. Boos, V. Bunichev, M. Dubinin⁴³, L. Dudko, A. Ershov, A. Gribushin, V. Klyukhin, O. Kodolova, I. Lokhtin, S. Obraztsov, V. Savrin

Novosibirsk State University (NSU), Novosibirsk, Russia

A. Barnyakov⁴⁴, V. Blinov⁴⁴, T. Dimova⁴⁴, L. Kardapol'tsev⁴⁴, Y. Skovpen⁴⁴

Institute for High Energy Physics of National Research Centre 'Kurchatov Institute', Protvino, Russia

I. Azhgirey, I. Bayshev, S. Bitioukov, V. Kachanov, D. Konstantinov, P. Mandrik, V. Petrov, R. Ryutin, S. Slabospitskii, A. Sobol, S. Troshin, N. Tyurin, A. Uzunian, A. Volkov

National Research Tomsk Polytechnic University, Tomsk, Russia

A. Babaev, A. Iuzhakov, V. Okhotnikov

Tomsk State University, Tomsk, Russia

V. Borchsh, V. Ivanchenko, E. Tcherniaev

University of Belgrade: Faculty of Physics and VINCA Institute of Nuclear Sciences

P. Adzic⁴⁵, P. Cirkovic, M. Dordevic, P. Milenovic, J. Milosevic, M. Stojanovic

Centro de Investigaciones Energéticas Medioambientales y Tecnológicas (CIEMAT), Madrid, Spain

M. Aguilar-Benitez, J. Alcaraz Maestre, A. Álvarez Fernández, I. Bachiller, M. Barrio Luna, Cristina F. Bedoya, J.A. Brochero Cifuentes, C.A. Carrillo Montoya, M. Cepeda, M. Cerrada, N. Colino, B. De La Cruz, A. Delgado Peris, J.P. Fernández Ramos, J. Flix, M.C. Fouz, O. Gonzalez Lopez, S. Goy Lopez, J.M. Hernandez, M.I. Josa, D. Moran, Á. Navarro Tobar, A. Pérez-Calero Yzquierdo, J. Puerta Pelayo, I. Redondo, L. Romero, S. Sánchez Navas, M.S. Soares, A. Triossi, C. Willmott

Universidad Autónoma de Madrid, Madrid, Spain

C. Albajar, J.F. de Trocóniz, R. Reyes-Almanza

Universidad de Oviedo, Instituto Universitario de Ciencias y Tecnologías Espaciales de Asturias (ICTEA), Oviedo, Spain

B. Alvarez Gonzalez, J. Cuevas, C. Erice, J. Fernandez Menendez, S. Folgueras, I. Gonzalez Caballero, J.R. González Fernández, E. Palencia Cortezon, V. Rodríguez Bouza, S. Sanchez Cruz

Instituto de Física de Cantabria (IFCA), CSIC-Universidad de Cantabria, Santander, Spain

I.J. Cabrillo, A. Calderon, B. Chazin Quero, J. Duarte Campderros, M. Fernandez,

P.J. Fernández Manteca, A. García Alonso, G. Gomez, C. Martinez Rivero, P. Martinez Ruiz del Arbol, F. Matorras, J. Piedra Gomez, C. Prieels, T. Rodrigo, A. Ruiz-Jimeno, L. Russo⁴⁶, L. Scodellaro, I. Vila, J.M. Vizan Garcia

University of Colombo, Colombo, Sri Lanka

K. Malagalage

University of Ruhuna, Department of Physics, Matara, Sri Lanka

W.G.D. Dharmaratna, N. Wickramage

CERN, European Organization for Nuclear Research, Geneva, Switzerland

D. Abbaneo, B. Akgun, E. Auffray, G. Auzinger, J. Baechler, P. Baillon, A.H. Ball, D. Barney, J. Bendavid, M. Bianco, A. Bocci, P. Bortignon, E. Bossini, E. Brondolin, T. Camporesi, A. Caratelli, G. Cerminara, E. Chapon, G. Cucciati, D. d'Enterria, A. Dabrowski, N. Daci, V. Daponte, A. David, O. Davignon, A. De Roeck, M. Deile, M. Dobson, M. Dünser, N. Dupont, A. Elliott-Peisert, N. Emriskova, F. Fallavollita⁴⁷, D. Fasanella, S. Fiorendi, G. Franzoni, J. Fulcher, W. Funk, S. Giani, D. Gigi, K. Gill, F. Glege, L. Gouskos, M. Gruchala, M. Guilbaud, D. Gulhan, J. Hegeman, C. Heidegger, Y. Iiyama, V. Innocente, T. James, P. Janot, O. Karacheban¹⁹, J. Kaspar, J. Kieseler, M. Krammer¹, N. Kratochwil, C. Lange, P. Lecoq, C. Lourenço, L. Malgeri, M. Mannelli, A. Massironi, F. Meijers, S. Mersi, E. Meschi, F. Moortgat, M. Mulders, J. Ngadiuba, J. Niedziela, S. Nourbakhsh, S. Orfanelli, L. Orsini, F. Pantaleo¹⁶, L. Pape, E. Perez, M. Peruzzi, A. Petrilli, G. Petrucciani, A. Pfeiffer, M. Pierini, F.M. Pitters, D. Rabady, A. Racz, M. Rieger, M. Rovere, H. Sakulin, J. Salfeld-Nebgen, C. Schäfer, C. Schwick, M. Selvaggi, A. Sharma, P. Silva, W. Snoeys, P. Sphicas⁴⁸, J. Steggemann, S. Summers, V.R. Tavolaro, D. Treille, A. Tsirou, G.P. Van Onsem, A. Vartak, M. Verzetti, W.D. Zeuner

Paul Scherrer Institut, Villigen, Switzerland

L. Caminada⁴⁹, K. Deiters, W. Erdmann, R. Horisberger, Q. Ingram, H.C. Kaestli, D. Kotlinski, U. Langenegger, T. Rohe, S.A. Wiederkehr

ETH Zurich - Institute for Particle Physics and Astrophysics (IPA), Zurich, Switzerland

M. Backhaus, P. Berger, N. Chernyavskaya, G. Dissertori, M. Dittmar, M. Donegà, C. Dorfer, T.A. Gómez Espinosa, C. Grab, D. Hits, W. Lusterhmann, R.A. Manzoni, M.T. Meinhard, F. Micheli, P. Musella, F. Nessi-Tedaldi, F. Pauss, G. Perrin, L. Perrozzi, S. Pigazzini, M.G. Ratti, M. Reichmann, C. Reissel, T. Reitenspiess, B. Ristic, D. Ruini, D.A. Sanz Becerra, M. Schönenberger, L. Shchutska, M.L. Vesterbacka Olsson, R. Wallny, D.H. Zhu

Universität Zürich, Zurich, Switzerland

T.K. Aarrestad, C. Amsler⁵⁰, C. Botta, D. Brzhechko, M.F. Canelli, A. De Cosa, R. Del Burgo, B. Kilminster, S. Leontsinis, V.M. Mikuni, I. Neutelings, G. Rauco, P. Robmann, K. Schweiger, C. Seitz, Y. Takahashi, S. Wertz, A. Zucchetta

National Central University, Chung-Li, Taiwan

T.H. Doan, C.M. Kuo, W. Lin, A. Roy, S.S. Yu

National Taiwan University (NTU), Taipei, Taiwan

P. Chang, Y. Chao, K.F. Chen, P.H. Chen, W.-S. Hou, Y.y. Li, R.-S. Lu, E. Paganis, A. Psallidas, A. Steen

Chulalongkorn University, Faculty of Science, Department of Physics, Bangkok, Thailand

B. Asavapibhop, C. Asawatangtrakuldee, N. Srimanobhas, N. Suwonjandee

Çukurova University, Physics Department, Science and Art Faculty, Adana, Turkey

A. Bat, F. Boran, A. Celik⁵¹, S. Damarseckin⁵², Z.S. Demiroglu, F. Dolek, C. Dozen⁵³,

I. Dumanoglu, G. Gokbulut, EmineGurpinar Guler⁵⁴, Y. Guler, I. Hos⁵⁵, C. Isik, E.E. Kangal⁵⁶, O. Kara, A. Kayis Topaksu, U. Kiminsu, G. Onengut, K. Ozdemir⁵⁷, S. Ozturk⁵⁸, A.E. Simsek, U.G. Tok, S. Turkcapar, I.S. Zorbakir, C. Zorbilmez

Middle East Technical University, Physics Department, Ankara, Turkey

B. Isildak⁵⁹, G. Karapinar⁶⁰, M. Yalvac

Bogazici University, Istanbul, Turkey

I.O. Atakisi, E. Gülmez, M. Kaya⁶¹, O. Kaya⁶², Ö. Özçelik, S. Tekten, E.A. Yetkin⁶³

Istanbul Technical University, Istanbul, Turkey

A. Cakir, K. Cankocak, Y. Komurcu, S. Sen⁶⁴

Istanbul University, Istanbul, Turkey

S. Cerci⁶⁵, B. Kaynak, S. Ozkorucuklu, D. Sunar Cerci⁶⁵

Institute for Scintillation Materials of National Academy of Science of Ukraine, Kharkov, Ukraine

B. Grynyov

National Scientific Center, Kharkov Institute of Physics and Technology, Kharkov, Ukraine

L. Levchuk

University of Bristol, Bristol, United Kingdom

E. Bhal, S. Bologna, J.J. Brooke, D. Burns⁶⁶, E. Clement, D. Cussans, H. Flacher, J. Goldstein, G.P. Heath, H.F. Heath, L. Kreczko, B. Krikler, S. Paramesvaran, B. Penning, T. Sakuma, S. Seif El Nasr-Storey, V.J. Smith, J. Taylor, A. Titterton

Rutherford Appleton Laboratory, Didcot, United Kingdom

K.W. Bell, A. Belyaev⁶⁷, C. Brew, R.M. Brown, D.J.A. Cockerill, J.A. Coughlan, K. Harder, S. Harper, J. Linacre, K. Manolopoulos, D.M. Newbold, E. Olaiya, D. Petyt, T. Reis, T. Schuh, C.H. Shepherd-Themistocleous, A. Thea, I.R. Tomalin, T. Williams

Imperial College, London, United Kingdom

R. Bainbridge, P. Bloch, J. Borg, S. Breeze, O. Buchmuller, A. Bundock, GurpreetSingh CHAHAL⁶⁸, D. Colling, P. Dauncey, G. Davies, M. Della Negra, R. Di Maria, P. Everaerts, G. Hall, G. Iles, M. Komm, L. Lyons, A.-M. Magnan, S. Malik, A. Martelli, V. Milosevic, A. Morton, J. Nash⁶⁹, V. Palladino, M. Pesaresi, D.M. Raymond, A. Richards, A. Rose, E. Scott, C. Seez, A. Shtipliyski, M. Stoye, T. Strebler, A. Tapper, K. Uchida, T. Virdee¹⁶, N. Wardle, D. Winterbottom, A.G. Zecchinelli, S.C. Zenz

Brunel University, Uxbridge, United Kingdom

J.E. Cole, P.R. Hobson, A. Khan, P. Kyberd, C.K. Mackay, I.D. Reid, L. Teodorescu, S. Zahid

Baylor University, Waco, USA

K. Call, B. Caraway, J. Dittmann, K. Hatakeyama, C. Madrid, B. McMaster, N. Pastika, C. Smith

Catholic University of America, Washington, DC, USA

R. Bartek, A. Dominguez, R. Uniyal, A.M. Vargas Hernandez

The University of Alabama, Tuscaloosa, USA

A. Buccilli, S.I. Cooper, C. Henderson, P. Rumerio, C. West

Boston University, Boston, USA

A. Albert, D. Arcaro, Z. Demiragli, D. Gastler, C. Richardson, J. Rohlf, D. Sperka, D. Spitzbart, I. Suarez, L. Sulak, D. Zou

Brown University, Providence, USA

G. Benelli, B. Burkley, X. Coubez¹⁷, D. Cutts, Y.t. Duh, M. Hadley, U. Heintz, J.M. Hogan⁷⁰, K.H.M. Kwok, E. Laird, G. Landsberg, K.T. Lau, J. Lee, M. Narain, S. Sagir⁷¹, R. Syarif, E. Usai, W.Y. Wong, D. Yu, W. Zhang

University of California, Davis, Davis, USA

R. Band, C. Brainerd, R. Breedon, M. Calderon De La Barca Sanchez, M. Chertok, J. Conway, R. Conway, P.T. Cox, R. Erbacher, C. Flores, G. Funk, F. Jensen, W. Ko[†], O. Kukral, R. Lander, M. Mulhearn, D. Pellett, J. Pilot, M. Shi, D. Taylor, K. Tos, M. Tripathi, Z. Wang, F. Zhang

University of California, Los Angeles, USA

M. Bachtis, C. Bravo, R. Cousins, A. Dasgupta, A. Florent, J. Hauser, M. Ignatenko, N. Mccoll, W.A. Nash, S. Regnard, D. Saltzberg, C. Schnaible, B. Stone, V. Valuev

University of California, Riverside, Riverside, USA

K. Burt, Y. Chen, R. Clare, J.W. Gary, S.M.A. Ghiasi Shirazi, G. Hanson, G. Karapostoli, O.R. Long, M. Olmedo Negrete, M.I. Paneva, W. Si, L. Wang, S. Wimpenny, B.R. Yates, Y. Zhang

University of California, San Diego, La Jolla, USA

J.G. Branson, P. Chang, S. Cittolin, S. Cooperstein, N. Deelen, M. Derdzinski, R. Gerosa, D. Gilbert, B. Hashemi, D. Klein, V. Krutelyov, J. Letts, M. Masciovecchio, S. May, S. Padhi, M. Pieri, V. Sharma, M. Tadel, F. Würthwein, A. Yagil, G. Zevi Della Porta

University of California, Santa Barbara - Department of Physics, Santa Barbara, USA

N. Amin, R. Bhandari, C. Campagnari, M. Citron, A. Dorsett, V. Dutta, M. Franco Sevilla, J. Incandela, B. Marsh, H. Mei, A. Ovcharova, H. Qu, J. Richman, U. Sarica, D. Stuart, S. Wang

California Institute of Technology, Pasadena, USA

D. Anderson, A. Bornheim, O. Cerri, I. Dutta, J.M. Lawhorn, N. Lu, J. Mao, H.B. Newman, T.Q. Nguyen, J. Pata, M. Spiropulu, J.R. Vlimant, S. Xie, Z. Zhang, R.Y. Zhu

Carnegie Mellon University, Pittsburgh, USA

M.B. Andrews, T. Ferguson, T. Mudholkar, M. Paulini, M. Sun, I. Vorobiev, M. Weinberg

University of Colorado Boulder, Boulder, USA

J.P. Cumalat, W.T. Ford, E. MacDonald, T. Mulholland, R. Patel, A. Perloff, K. Stenson, K.A. Ulmer, S.R. Wagner

Cornell University, Ithaca, USA

J. Alexander, Y. Cheng, J. Chu, A. Datta, A. Frankenthal, K. Mcdermott, J.R. Patterson, D. Quach, A. Ryd, S.M. Tan, Z. Tao, J. Thom, P. Wittich, M. Zientek

Fermi National Accelerator Laboratory, Batavia, USA

S. Abdullin, M. Albrow, M. Alyari, G. Apollinari, A. Apresyan, A. Apyan, S. Banerjee, L.A.T. Bauerdick, A. Beretvas, D. Berry, J. Berryhill, P.C. Bhat, K. Burkett, J.N. Butler, A. Canepa, G.B. Cerati, H.W.K. Cheung, F. Chlebana, M. Cremonesi, J. Duarte, V.D. Elvira, J. Freeman, Z. Gecse, E. Gottschalk, L. Gray, D. Green, S. Grünendahl, O. Gutsche, J. Hanlon, R.M. Harris, S. Hasegawa, R. Heller, J. Hirschauer, B. Jayatilaka, S. Jindariani, M. Johnson, U. Joshi, T. Klijnsma, B. Klima, M.J. Kortelainen, B. Kreis, S. Lammel, J. Lewis, D. Lincoln, R. Lipton, M. Liu, T. Liu, J. Lykken, K. Maeshima, J.M. Marraffino, D. Mason, P. McBride, P. Merkel, S. Mrenna, S. Nahn, V. O'Dell, V. Papadimitriou, K. Pedro, C. Pena, G. Rakness, F. Ravera, A. Reinsvold Hall, L. Ristori, B. Schneider, E. Sexton-Kennedy, N. Smith, A. Soha, W.J. Spalding, L. Spiegel, S. Stoynev, J. Strait, N. Strobbe, L. Taylor, S. Tkaczyk, N.V. Tran, L. Uplegger, E.W. Vaandering, C. Vernieri, R. Vidal, M. Wang, H.A. Weber

University of Florida, Gainesville, USA

D. Acosta, P. Avery, D. Bourilkov, A. Brinkerhoff, L. Cadamuro, V. Cherepanov, F. Errico, R.D. Field, S.V. Gleyzer, D. Guerrero, B.M. Joshi, M. Kim, J. Konigsberg, A. Korytov, K.H. Lo, K. Matchev, N. Menendez, G. Mitselmakher, D. Rosenzweig, K. Shi, J. Wang, S. Wang, X. Zuo

Florida International University, Miami, USA

Y.R. Joshi

Florida State University, Tallahassee, USA

T. Adams, A. Askew, S. Hagopian, V. Hagopian, K.F. Johnson, R. Khurana, T. Kolberg, G. Martinez, T. Perry, H. Prosper, C. Schiber, R. Yohay, J. Zhang

Florida Institute of Technology, Melbourne, USA

M.M. Baarmand, M. Hohlmann, D. Noonan, M. Rahmani, M. Saunders, F. Yumiceva

University of Illinois at Chicago (UIC), Chicago, USA

M.R. Adams, L. Apanasevich, R.R. Betts, R. Cavanaugh, X. Chen, S. Dittmer, O. Evdokimov, C.E. Gerber, D.A. Hangal, D.J. Hofman, C. Mills, T. Roy, M.B. Tonjes, N. Varelas, J. Viinikainen, H. Wang, X. Wang, Z. Wu

The University of Iowa, Iowa City, USA

M. Alhuseini, B. Bilki⁵⁴, K. Dilsiz⁷², S. Durgut, R.P. Gandrajula, M. Haytmyradov, V. Khristenko, O.K. Köseyan, J.-P. Merlo, A. Mestvirishvili⁷³, A. Moeller, J. Nachtman, H. Ogul⁷⁴, Y. Onel, F. Ozok⁷⁵, A. Penzo, C. Snyder, E. Tiras, J. Wetzel

Johns Hopkins University, Baltimore, USA

B. Blumenfeld, A. Cocoros, N. Eminizer, A.V. Gritsan, W.T. Hung, S. Kyriacou, P. Maksimovic, J. Roskes, M. Swartz

The University of Kansas, Lawrence, USA

C. Baldenegro Barrera, P. Baringer, A. Bean, S. Boren, J. Bowen, A. Bylinkin, T. Isidori, S. Khalil, J. King, G. Krintiras, A. Kropivnitskaya, C. Lindsey, D. Majumder, W. Mcbrayer, N. Minafra, M. Murray, C. Rogan, C. Royon, S. Sanders, E. Schmitz, J.D. Tapia Takaki, Q. Wang, J. Williams, G. Wilson

Kansas State University, Manhattan, USA

S. Duric, A. Ivanov, K. Kaadze, D. Kim, Y. Maravin, D.R. Mendis, T. Mitchell, A. Modak, A. Mohammadi

Lawrence Livermore National Laboratory, Livermore, USA

F. Rebassoo, D. Wright

University of Maryland, College Park, USA

A. Baden, O. Baron, A. Belloni, S.C. Eno, Y. Feng, N.J. Hadley, S. Jabeen, G.Y. Jeng, R.G. Kellogg, A.C. Mignerey, S. Nabili, F. Ricci-Tam, M. Seidel, Y.H. Shin, A. Skuja, S.C. Tonwar, K. Wong

Massachusetts Institute of Technology, Cambridge, USA

D. Abercrombie, B. Allen, A. Baty, R. Bi, S. Brandt, W. Busza, I.A. Cali, M. D'Alfonso, G. Gomez Ceballos, M. Goncharov, P. Harris, D. Hsu, M. Hu, M. Klute, D. Kovalskyi, Y.-J. Lee, P.D. Luckey, B. Maier, A.C. Marini, C. Mcginn, C. Mironov, S. Narayanan, X. Niu, C. Paus, D. Rankin, C. Roland, G. Roland, Z. Shi, G.S.F. Stephens, K. Sumorok, K. Tatar, D. Velicanu, J. Wang, T.W. Wang, B. Wyslouch

University of Minnesota, Minneapolis, USA

R.M. Chatterjee, A. Evans, S. Guts[†], P. Hansen, J. Hiltbrand, Sh. Jain, Y. Kubota, Z. Lesko, J. Mans, M. Revering, R. Rusack, R. Saradhy, N. Schroeder, M.A. Wadud

University of Mississippi, Oxford, USA

J.G. Acosta, S. Oliveros

University of Nebraska-Lincoln, Lincoln, USA

K. Bloom, S. Chauhan, D.R. Claes, C. Fangmeier, L. Finco, F. Golf, R. Kamalieddin, I. Kravchenko, J.E. Siado, G.R. Snow[†], B. Stieger, W. Tabb

State University of New York at Buffalo, Buffalo, USA

G. Agarwal, C. Harrington, I. Iashvili, A. Kharchilava, C. McLean, D. Nguyen, A. Parker, J. Pekkanen, S. Rappoccio, B. Roozbahani

Northeastern University, Boston, USA

G. Alverson, E. Barberis, C. Freer, Y. Haddad, A. Hortiangtham, G. Madigan, B. Marzocchi, D.M. Morse, T. Orimoto, L. Skinnari, A. Tishelman-Charny, T. Wamorkar, B. Wang, A. Wisecarver, D. Wood

Northwestern University, Evanston, USA

S. Bhattacharya, J. Bueghly, A. Gilbert, T. Gunter, K.A. Hahn, N. Odell, M.H. Schmitt, K. Sung, M. Trovato, M. Velasco

University of Notre Dame, Notre Dame, USA

R. Bucci, N. Dev, R. Goldouzian, M. Hildreth, K. Hurtado Anampa, C. Jessop, D.J. Karmgard, K. Lannon, W. Li, N. Loukas, N. Marinelli, I. Mcalister, F. Meng, Y. Musienko³⁷, R. Ruchti, P. Siddireddy, G. Smith, S. Taroni, M. Wayne, A. Wightman, M. Wolf, A. Woodard

The Ohio State University, Columbus, USA

J. Alimena, B. Bylsma, L.S. Durkin, B. Francis, C. Hill, W. Ji, A. Lefeld, T.Y. Ling, B.L. Winer

Princeton University, Princeton, USA

G. Dezoort, P. Elmer, J. Hardenbrook, N. Haubrich, S. Higginbotham, A. Kalogeropoulos, S. Kwan, D. Lange, M.T. Lucchini, J. Luo, D. Marlow, K. Mei, I. Ojalvo, J. Olsen, C. Palmer, P. Piroué, D. Stickland, C. Tully

University of Puerto Rico, Mayaguez, USA

S. Malik, S. Norberg

Purdue University, West Lafayette, USA

A. Barker, V.E. Barnes, R. Chawla, S. Das, L. Gutay, M. Jones, A.W. Jung, A. Khatiwada, B. Mahakud, D.H. Miller, G. Negro, N. Neumeister, C.C. Peng, S. Piperov, H. Qiu, J.F. Schulte, N. Trevisani, F. Wang, R. Xiao, W. Xie

Purdue University Northwest, Hammond, USA

T. Cheng, J. Dolen, N. Parashar

Rice University, Houston, USA

U. Behrens, S. Dildick, K.M. Ecklund, S. Freed, F.J.M. Geurts, M. Kilpatrick, Arun Kumar, W. Li, B.P. Padley, R. Redjimi, J. Roberts, J. Rorie, W. Shi, A.G. Stahl Leiton, Z. Tu, A. Zhang

University of Rochester, Rochester, USA

A. Bodek, P. de Barbaro, R. Demina, J.L. Dulemba, C. Fallon, T. Ferbel, M. Galanti, A. Garcia-Bellido, O. Hindrichs, A. Khukhunaishvili, E. Ranken, R. Taus

Rutgers, The State University of New Jersey, Piscataway, USA

B. Chiarito, J.P. Chou, A. Gandrakota, Y. Gershtein, E. Halkiadakis, A. Hart, M. Heindl, E. Hughes, S. Kaplan, I. Laflotte, A. Lath, R. Montalvo, K. Nash, M. Osherson, H. Saka, S. Salur, S. Schnetzer, S. Somalwar, R. Stone, S. Thomas

University of Tennessee, Knoxville, USA

H. Acharya, A.G. Delannoy, S. Spanier

Texas A&M University, College Station, USA

O. Bouhali⁷⁶, M. Dalchenko, M. De Mattia, A. Delgado, R. Eusebi, J. Gilmore, T. Huang, T. Kamon⁷⁷, H. Kim, S. Luo, S. Malhotra, D. Marley, R. Mueller, D. Overton, L. Perniè, D. Rathjens, A. Safonov

Texas Tech University, Lubbock, USA

N. Akchurin, J. Damgov, F. De Guio, V. Hegde, S. Kunori, K. Lamichhane, S.W. Lee, T. Mengke, S. Muthumuni, T. Peltola, S. Undleeb, I. Volobouev, Z. Wang, A. Whitbeck

Vanderbilt University, Nashville, USA

S. Greene, A. Gurrola, R. Janjam, W. Johns, C. Maguire, A. Melo, H. Ni, K. Padeken, F. Romeo, P. Sheldon, S. Tuo, J. Velkovska, M. Verweij

University of Virginia, Charlottesville, USA

M.W. Arenton, P. Barria, B. Cox, G. Cummings, J. Hakala, R. Hirosky, M. Joyce, A. Ledovskoy, C. Neu, B. Tannenwald, Y. Wang, E. Wolfe, F. Xia

Wayne State University, Detroit, USA

R. Harr, P.E. Karchin, N. Poudyal, J. Sturdy, P. Thapa

University of Wisconsin - Madison, Madison, WI, USA

T. Bose, J. Buchanan, C. Caillol, D. Carlsmith, S. Dasu, I. De Bruyn, L. Dodd, C. Galloni, H. He, M. Herndon, A. Hervé, U. Hussain, A. Lanaro, A. Loeliger, K. Long, R. Loveless, J. Madhusudanan Sreekala, A. Mallampalli, D. Pinna, T. Ruggles, A. Savin, V. Sharma, W.H. Smith, D. Teague, S. Trembath-reichert

†: Deceased

1: Also at Vienna University of Technology, Vienna, Austria

2: Also at IRFU, CEA, Université Paris-Saclay, Gif-sur-Yvette, France

3: Also at Universidade Estadual de Campinas, Campinas, Brazil

4: Also at Federal University of Rio Grande do Sul, Porto Alegre, Brazil

5: Also at UFMS, Nova Andradina, Brazil

6: Also at Universidade Federal de Pelotas, Pelotas, Brazil

7: Also at Université Libre de Bruxelles, Bruxelles, Belgium

8: Also at University of Chinese Academy of Sciences, Beijing, China

9: Also at Institute for Theoretical and Experimental Physics named by A.I. Alikhanov of NRC 'Kurchatov Institute', Moscow, Russia

10: Also at Joint Institute for Nuclear Research, Dubna, Russia

11: Also at Cairo University, Cairo, Egypt

12: Also at Zewail City of Science and Technology, Zewail, Egypt

13: Also at Purdue University, West Lafayette, USA

14: Also at Université de Haute Alsace, Mulhouse, France

15: Also at Erzincan Binali Yildirim University, Erzincan, Turkey

16: Also at CERN, European Organization for Nuclear Research, Geneva, Switzerland

17: Also at RWTH Aachen University, III. Physikalisches Institut A, Aachen, Germany

- 18: Also at University of Hamburg, Hamburg, Germany
- 19: Also at Brandenburg University of Technology, Cottbus, Germany
- 20: Also at Institute of Physics, University of Debrecen, Debrecen, Hungary, Debrecen, Hungary
- 21: Also at Institute of Nuclear Research ATOMKI, Debrecen, Hungary
- 22: Also at MTA-ELTE Lendület CMS Particle and Nuclear Physics Group, Eötvös Loránd University, Budapest, Hungary, Budapest, Hungary
- 23: Also at IIT Bhubaneswar, Bhubaneswar, India, Bhubaneswar, India
- 24: Also at Institute of Physics, Bhubaneswar, India
- 25: Also at Shoolini University, Solan, India
- 26: Also at University of Hyderabad, Hyderabad, India
- 27: Also at University of Visva-Bharati, Santiniketan, India
- 28: Also at Isfahan University of Technology, Isfahan, Iran
- 29: Now at INFN Sezione di Bari ^a, Università di Bari ^b, Politecnico di Bari ^c, Bari, Italy
- 30: Also at Italian National Agency for New Technologies, Energy and Sustainable Economic Development, Bologna, Italy
- 31: Also at Centro Siciliano di Fisica Nucleare e di Struttura Della Materia, Catania, Italy
- 32: Also at Scuola Normale e Sezione dell'INFN, Pisa, Italy
- 33: Also at Riga Technical University, Riga, Latvia, Riga, Latvia
- 34: Also at Malaysian Nuclear Agency, MOSTI, Kajang, Malaysia
- 35: Also at Consejo Nacional de Ciencia y Tecnología, Mexico City, Mexico
- 36: Also at Warsaw University of Technology, Institute of Electronic Systems, Warsaw, Poland
- 37: Also at Institute for Nuclear Research, Moscow, Russia
- 38: Now at National Research Nuclear University 'Moscow Engineering Physics Institute' (MEPhI), Moscow, Russia
- 39: Also at St. Petersburg State Polytechnical University, St. Petersburg, Russia
- 40: Also at University of Florida, Gainesville, USA
- 41: Also at Imperial College, London, United Kingdom
- 42: Also at P.N. Lebedev Physical Institute, Moscow, Russia
- 43: Also at California Institute of Technology, Pasadena, USA
- 44: Also at Budker Institute of Nuclear Physics, Novosibirsk, Russia
- 45: Also at Faculty of Physics, University of Belgrade, Belgrade, Serbia
- 46: Also at Università degli Studi di Siena, Siena, Italy
- 47: Also at INFN Sezione di Pavia ^a, Università di Pavia ^b, Pavia, Italy, Pavia, Italy
- 48: Also at National and Kapodistrian University of Athens, Athens, Greece
- 49: Also at Universität Zürich, Zurich, Switzerland
- 50: Also at Stefan Meyer Institute for Subatomic Physics, Vienna, Austria, Vienna, Austria
- 51: Also at Burdur Mehmet Akif Ersoy University, BURDUR, Turkey
- 52: Also at Şırnak University, Sirnak, Turkey
- 53: Also at Department of Physics, Tsinghua University, Beijing, China, Beijing, China
- 54: Also at Beykent University, Istanbul, Turkey, Istanbul, Turkey
- 55: Also at Istanbul Aydin University, Application and Research Center for Advanced Studies (App. & Res. Cent. for Advanced Studies), Istanbul, Turkey
- 56: Also at Mersin University, Mersin, Turkey
- 57: Also at Piri Reis University, Istanbul, Turkey
- 58: Also at Gaziosmanpasa University, Tokat, Turkey
- 59: Also at Ozyegin University, Istanbul, Turkey
- 60: Also at Izmir Institute of Technology, Izmir, Turkey
- 61: Also at Marmara University, Istanbul, Turkey

- 62: Also at Kafkas University, Kars, Turkey
- 63: Also at Istanbul Bilgi University, Istanbul, Turkey
- 64: Also at Hacettepe University, Ankara, Turkey
- 65: Also at Adiyaman University, Adiyaman, Turkey
- 66: Also at Vrije Universiteit Brussel, Brussel, Belgium
- 67: Also at School of Physics and Astronomy, University of Southampton, Southampton, United Kingdom
- 68: Also at IPPP Durham University, Durham, United Kingdom
- 69: Also at Monash University, Faculty of Science, Clayton, Australia
- 70: Also at Bethel University, St. Paul, Minneapolis, USA, St. Paul, USA
- 71: Also at Karamanoğlu Mehmetbey University, Karaman, Turkey
- 72: Also at Bingol University, Bingol, Turkey
- 73: Also at Georgian Technical University, Tbilisi, Georgia
- 74: Also at Sinop University, Sinop, Turkey
- 75: Also at Mimar Sinan University, Istanbul, Istanbul, Turkey
- 76: Also at Texas A&M University at Qatar, Doha, Qatar
- 77: Also at Kyungpook National University, Daegu, Korea, Daegu, Korea